energies

MDPI

Review

Recent Advances in the Critical Heat Flux Amelioration of Pool Boiling Surfaces Using Metal Oxide Nanoparticle Deposition

Hesam Moghadasi [1], Navid Malekian [1], Hamid Saffari [1], Amir Mirza Gheitaghy [2,*] and Guo Qi Zhang [2]

[1] School of Mechanical Engineering, Iran University of Science and Technology, Tehran 16846-13114, Iran; hesam_moghadasi@mecheng.iust.ac.ir (H.M.); navid.malekian@yahoo.com (N.M.); saffari@iust.ac.ir (H.S.)
[2] Department of Microelectronics, Delft University of Technology, 2628 CD Delft, The Netherlands; G.Q.Zhang@tudelft.nl
* Correspondence: a.mirzagheytaghi@tudelft.nl

Received: 28 June 2020; Accepted: 29 July 2020; Published: 4 August 2020

Abstract: Pool boiling is an effective heat transfer process in a wide range of applications related to energy conversion, including power generation, solar collectors, cooling systems, refrigeration and air conditioning. By considering the broad range of applications, any improvement in higher heat-removal yield can ameliorate the ultimate heat usage and delay or even avoid the occurrence of system failures, thus leading to remarkable economic, environmental and energy efficiency outcomes. A century of research on ameliorating critical heat flux (CHF) has focused on altering the boiling surface characteristics, such as its nucleation site density, wettability, wickability and heat transfer area, by many innovative techniques. Due to the remarkable interest of using nanoparticle deposition on boiling surfaces, this review is targeted towards investigating whether or not metal oxide nanoparticles can modify surface characteristics to enhance the CHF. The influence of nanoparticle material, thermo-physical properties, concentration, shape, and size are categorized, and the inconsistency or contradictions of the existing research results are recognized. In the following, nanoparticle deposition methods are presented to provide a worthwhile alternative to deposition rather than nanofluid boiling. Furthermore, possible mechanisms and models are identified to explain the amelioration results. Finally, the present status of nanoparticle deposition for CHF amelioration, along with their future challenges, amelioration potentials, limitations, and their possible industrial implementation, is discussed.

Keywords: critical heat flux; pool boiling; metal oxide; nanoparticle deposition; energy conversion

1. Introduction

1.1. Pool Boiling Phenomenon

Pool boiling is proposed as a beneficial method for the transfer of high thermal energy in various applications of industry, such as refrigeration, cooling electronic chips as well as nuclear reactor cooling, the generation of thermal power and the conversion of energy. Regarding to the widespread use of this process in different fields, understanding the origin, process and existing developments in this field is of valuable importance [1,2]. In the pool boiling process, the heating surface is submerged in a pool with a great amount of stagnant liquid. To study the influence of diverse parameters, including the behavior of heater surfaces in addition to the use of various fluids, several investigations have been conducted on a laboratory scale [3–5].

The boiling performance is mostly characterized by the use of two main parameters. These parameters are identified as HTC (heat transfer coefficient) and CHF (critical heat flux). HTC is a measure determining the rate of removed heat for a unit increase in the temperature of a heated surface. The latter parameter, CHF, is attributed to the upper limit of nucleate boiling. CHF is an important criterion, because, in higher heat fluxes, an insulating vapor film would be formed on the boiling surface, which may result in a catastrophic burnout, consequently. In addition, a significant HTC drop can occur as a consequence of CHF phenomenon, which is followed by a remarkable rise in surface temperature. Therefore, to enhance the boiling heat transfer, HTC should be maximized, which would lead to a growth in CHF. Considering the conditions and environments in which CHF happens, diverse titles can be utilized to refer to CHF, including boiling crisis, burnout heat flux, departure from nuclear boiling, or dryout. After CHF point, an abrupt decline would occur in the efficiency of the heat transfer and, therefore, localized overheating would be generated in the heated surface. Since there is a direct relationship between the boiling limit and physical burnout of the heated surface, keeping CHF in a credible limit is crucial for ensuring the safety of the system [6,7].

According to Figure 1, for the boiling heat transfer, the target is to maximize the permissible CHF limit as well as rising HTC that is defined by a local difference on the curve. Furthermore, a reduction in the needed thermal loads for the onset of nucleate boiling (ONB) is proposed as another important matter. ONB refers to a starting point, in which the phase-change in the heat dissipation from the single-phase convection heat transfer of the liquid occurs. A comparison of common and improved boiling curves is illustrated in Figure 1.

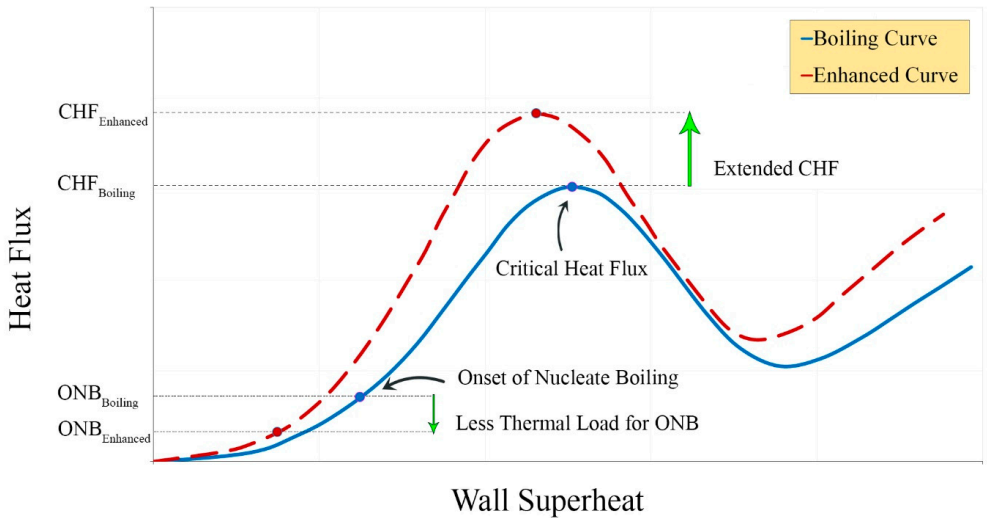

Figure 1. Comparison between common and ameliorated pool boiling curves.

1.2. CHF Importance in Energy Applications

CHF is a phenomenon relating to the point in which a persistent liquid contact cannot be preserved at the heated surface. Being thoroughly accurate, this special term shows the heat flux corresponding to the occurrence of the phenomenon. Among other terms that are often used are boiling crisis, departure from nucleate boiling (DNB), dryout and burnout. CHF is an interesting and substantial phenomenon from both fundamental and practical standpoints. From a fundamental viewpoint, CHF includes broad variations in heat transfer, pressure drop and flow regime. From the practical viewpoint, lots of application fields are in direct contact with CHF, including fusion applications, nuclear power plants, fossil power plants, steam generators and so on. In these fields, CHF notably affects the controllability, safety, efficiency, integrity and economic competitiveness of systems and subsystems [8].

CHF investigation is also precious in electronic cooling systems, fusion component heat removal, designing neutral particle beams to treat cancer patients, and removing heat from the blades of

high-temperature gas turbines [9]. Chio et al. [10] conducted CHF experiments in a three-rod bundle in a high-flux advanced neutron application reactor. So as to consider the geometric effect of the three-rod bundle, a three-pin correction factor was developed. An example of cooling electronic systems based on boiling mechanism utilizing PF-5060 dielectric liquid of high-power computer chips is exhibited, schematically, in Figure 2 in which the composite spreaders increased the total thermal power removed at relatively low chip temperature.

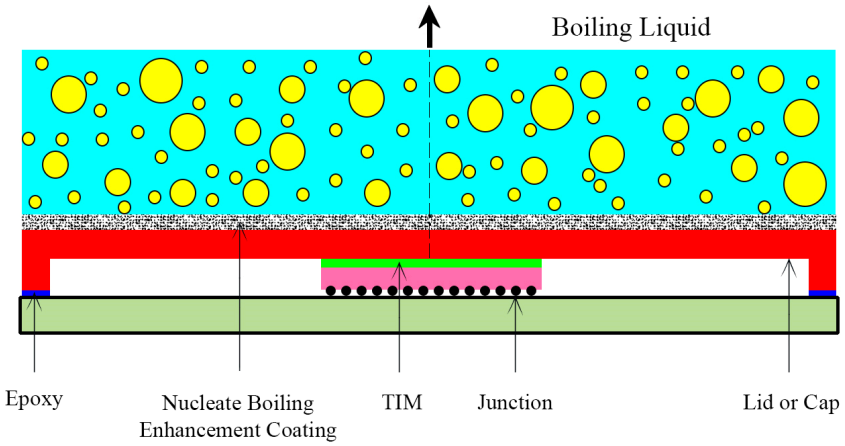

Figure 2. Application of pool boiling in systems utilized for cooling electronic chips.

Since vertical two-dimensional channels made of parallel plates are a frequently utilized element in thermal engineering facilities, Guo and Wu [11] systematically investigated thermal drag and CHF for natural convection of air in vertical channels. As an outcome, CHF may appear in the channel and the boiling process, because the possibility of heat transfer for the channel geometry is restricted. The following suggested correlation that can evaluate CHF presents a new criterion for thermal analysis and designing narrow-spaced equipment.

$$q_{w,cri} = 0.06 \frac{\rho_\infty C_P g b^3 T_\infty}{\nu_\infty l} \quad (1)$$

where $q_{w,cri}$, ρ_∞, C_P, g, b, T_∞, ν_∞ and l represent the critical heat flux, density of ambient fluid, specific heat capacity, gravitational acceleration, channel half-spacing, temperature of ambient fluid, kinematic viscosity of ambient fluid and channel height, respectively. Wu and Zhao [12] explored nanofluid heat transfer and CHF amelioration from the standpoint of a research gap in engineering applications. They expressed that the available empirical data of nanofluids' thermal characteristics are incomplete and invalid when engineering applications are considered to be important. To succeed in dealing with the research gaps for these applications, the suggested approaches include estimating nanofluid stability under quiescent and flow conditions, establishing a nanofluid database containing nanoparticle size, distribution and additives, which is helpful to advance the knowledge about the interaction of suspended nanoparticles and boundary layers. Hence, realizing convective heat transfer enhancement, and ultimately the empirical and numerical study of the bubble dynamics of boiling nanofluids, will be accessible.

Two-phase pressure drop, boiling heat transfer, and CHF to water were checked by Yu et al. [13] in small horizontal tubes installed in compact heat exchangers. It was pointed out that CHF occurred at relatively great qualities of water (between 0.5 and 1.0) in the horizontal channel being studied. These qualities are higher than those reported for large tubes (at higher pressures and mass fluxes). The CHF quality was concluded to decrease with mass flux reduction, while opposite behavior had been observed in large tubes.

Since enhancing CHF of industrial boilers through surface modification can result in vital energy savings and global reduction in greenhouse gas emissions, Dhillon et al. [14] scrutinized the influence of CHF maxima during boiling crisis on textured surfaces. They proposed a coupled thermal-hydraulic model that associates CHF amelioration with the rewetting of a hot dry spot on the boiling surface.

1.3. CHF Enhancement Methods

This section deals with CHF enhancement methods. According to the available literature, four general methods are proposed for enhancing CHF, including ameliorating fluid properties with nanoparticles, modifying surface characteristics, changing flow channel structures, and the integration of hybrid approaches that will be discussed in the following.

1.3.1. CHF Enhancement by Ameliorating Fluid Properties with Nanoparticles

Altering the working fluids can be considered as a primary way for CHF enhancement. Several research studies were conducted on the replacement of different fluids, including Freon-12 or Freon-134a with water in the early 1990s [15]. Improving the properties of the base fluid with nanoparticles is regarded as another useful solution of heat transfer enhancement. Nanofluids are a new category of heat transfer fluids, in which the stable suspending nanoparticles (with the approximate dimensions of 1–50 nm) are dispersed in common base fluids. Various fluids can be used as the base fluids, including water [16], refrigerant [17], or organic fluids [18]. among them, water, oil, ethylene, bio-fluids, and different polymer solutions can be mentioned. Moreover, nanoparticles can include diverse materials such as metals with chemical stability (copper, silver, gold), metal oxides (alumina, titania, silica, zirconia, bismuth oxide), carbon allotropes (diamond, fullerene, single-walled and multi-walled carbon nanotubes), as well as functionalized nanoparticles [19–23]. Even hybrid nanoparticles and nano-fluids can be used for heat transfer [24] and pool boiling enhancement [25,26]. Thus, it can be inferred that the CHF is enhanced by the modification of fluid properties through adding various particles to the base fluids [27,28].

1.3.2. CHF Enhancement by Modifying Surface Characteristics

Generally, surface characteristics can be improved by the deposition of the nanoparticles [29–31]. The heat transfer surface in pool boiling can be modified by uniform/modulated porous coatings and fabrication/installation of the diverse structures on the heated surface [32]. Different methods have been presented for the fabrication of surfaces with porous coating of uniform thickness, including welding, sintering, brazing of particles, flame spraying, electrolytic deposition, plating to bond of particle, galvanizing, plasma spraying of a polymer, metallic coating of a foam substrate, and the deposition of nanoparticles. In a different investigation, various processes have been implemented for producing a heater surface with enhanced CHF, including nano-wires [33,34], nano-porous structures [9,35], micro-porous surface layers [36,37], nano-tube arrays [28], carbon nano-tube coating [38,39] or composite porous surfaces [40].

Experimental studies on a modulated porous-layer coating revealed CHF enhancement about 2–3 times in comparison with a plain surface [41]. In some studies [42,43], innovative structures with separated paths of liquid and vapor were proposed as porous media. These separated paths may lead to a decline in flow resistance, which results in an enhancement in CHF. Further enhancement in CHF by micro-fabrication techniques can be achieved by the use of microstructures that are coated with zinc oxide nano-rods [44], silicon nanowires [45,46], sintered surface [47,48] and the tobacco mosaic virus [49].

1.3.3. CHF Enhancement by Changing Flow Channel Structures

Improving the structure of the flow passage is considered as an effective approach for CHF amelioration. The deposition of the nanoparticle affects the flow pattern of nanofluid in the vicinity of the structured surface. Through the machining of the micro-channels' surfaces, some bubbles may

be formed, grow and detach to inhibit the instability during the transformation into film boiling. In a study by Kandlikar [50], pool boiling was performed in a substrate with fins. According to the obtained results, it was observed that CHF value was 3 MW/cm^2 at a superheating temperature equal to 4.8 °C. However, this value was 1.25 MW/cm^2 at a higher superheating temperature of 17 °C in a plain surface. In another study, Boziuk et al. [51] achieved 218% CHF amelioration in comparison with the plain surface through the use of micro-channels. According to [52], expanding the cross-section is another way to modify the micro-channels. By the expansion angle in the range of 0–2°, a significant increase in CHF from 178 to 489 W/cm^2 can be achieved besides a low-pressure drop. In addition, Gheytaghi et al. [53] demonstrated the 65% increase in CHF with inclined micro-channels.

1.3.4. CHF Enhancement by Integration of Hybrid Approaches

Integration of the aforementioned approaches with the porous structures is regarded as an another approach for further CHF enhancement [54]. Bai et al. [55] explained the influence of a porous artery structure on the CHF enhancement. In their study, the environmental conditions for the buildup of capillary pressure was provided through the use of porous layers in the interface of liquid/vapor. This led to a movement of vapor venting through the artery to the side liquid rather than the upper bulk liquid. Thus, the possibility of phase transformation would be reduced during nucleation boiling. Three designs of porous coated surfaces were suggested by Joshi and Dede [56]. Moreover, jet orifices were used to evaluate the performance of two-phase flow. These designs included an open tunnel, a closed tunnel, and a pin-fin heat spreader on it. Among the three mentioned designs, the third design reached the best CHF of more than 218 W/cm^2, while the reported CHF for other designs was about 200 W/cm^2. Another example of a hybrid approach is the use of acoustic actuation, where interfacial forces would be induced, which motivates the detachment of the bubbles in a smaller scale and prevents the vapor buildup. It was reported that the integration of textured surface with acoustic actuation induced by a 1.7 MHz ultrasonic piezoelectric transducer [57] would lead to 65% and 30% CHF enhancement in plain and modified surfaces, respectively.

1.4. Previous Review Studies on CHF Enhancement

Lots of review papers have been issued in the field of enhancing heat transfer in pool boiling by surface modification. These papers can be categorized into two groups. In the first group, pool boiling was explored along with other heat transfer mechanisms. However, in the second group, pool boiling was studied exclusively. The investigations of Bergles et al. [58] and Webb et al. [59], in which 508 papers and reports as well as 59 U.S. patents were documented in the field of pool boiling and flow boiling prior to 1980 are classified in the first group. Furthermore, the studies of Bhavnani et al. [60], Shojaeian and Koşar [61], McCarthy et al. [62], Kim et al. [63], and Attinger et al. [64] are included in this group. Among the reviews focusing entirely on pool boiling enhancement, the paper of Honda and Wei [65] can be mentioned, which reported the studies for the improvement of cooling performance in electronic devices through the usage of surface microstructures prior to 2004. In another research, Lu and Kandlikar [66] reviewed the enhancement of pool boiling by using modification techniques for nanoscale surfaces. In addition, manufacturing methods for porous surfaces in pool boiling applications were reviewed by Patil and Kandlikar [67]. Moreover, Mori and Utaka [68] have recently published a review for the used techniques to CHF improvement in pool boiling. However, amelioration of HTC was not mentioned within the nucleate boiling region.

In a research study by Rioux et al. [69], nanostructure surfaces made by microscale acid etching through a sintering process were examined. Regarding their obtained results, the use of hierarchical multiscale modulated porous surfaces would lead to 200% augmentation in CHF in comparison with the polished plain surface. Silver-nanoparticles suspended in de-ionized water with plate heaters were scrutinized by Jo et al. [70]. They demonstrated the shift of boiling curves to the right side. Additionally, they inferred the CHF enhancement by the reduction in the nanoparticles size. Experimental studies on the surfaces of micro-channeled with micro-porous coatings were performed by Patil et al. [71] and

Jaikumar et al. [72] via diverse methodologies (sintering, electrodeposition, etc.). In these investigations, remarkable enhancements in CHF were observed. Sarafraz et al. [73] compared the thermal performance of pool boiling in alumina nano-fluid for both plain and micro-structured surfaces. They pointed out the augmented rate of CHF enhancement by increasing nanofluid mass concentration, nanoparticle size and interspace between microstructures. Nucleate pool boiling of Al_2O_3-based aqueous nanofluid was prospected by Shahmoradi et al. [74] on a flat plate heater. They declared that by increasing CHF, HTC of nanofluid experiences a descending trend. Moreover, they reported an increase in CHF amelioration by a rising volume fraction of nanoparticles. Jaikumar and Kandlikar [47] revealed different nucleating and non-nucleating regions, which facilitates the separation of liquid–vapor pathways for the detachment of the vapor bubbles and returning liquid that would lead to CHF enhancement.

Heat transfer improvement with surfactants and polymeric additives was addressed in the comprehensive reviews of Cheng et al. [75] and Wasekar and Manglik [76]. It is worth mentioning that the use of nanofluids for the CHF amelioration of both pool boiling and forced convection was listed in the recent reviews. In a review by Ciloglu and Bolukbasi [77], the investigations associated with pool boiling were listed up to 2015. In the mentioned review, it was aimed to justify the conflicting findings for nanofluids pool boiling. Other reviews regarding the pool boiling of nanofluids, such as Yu et al. [78], Li et al. [79], Özerinç et al. [80], Kleinstreuer and Feng [81], Ghadimi et al. [82], Saidur et al. [83], Ramesh and Prabhu [84], Yu and Xie [85], Mahian et al. [86], Sidik et al. [87], Haddad et al. [88], Shahrul et al. [89], Kasaeian et al. [90], and Devendiran and Amirtham [91], were concentrated on the preparation methods for nanofluid, instruments and methods for inspection, thermo-physical characteristics, as well as applications.

1.5. Nanoparticle Deposition Method

The deposition of nanoparticles is defined as the attachment of nanoparticles to the solid surfaces, which are called substrates, to form coatings of nanoparticles. The properties of different materials' surfaces will change if nanoparticles are deposed on them. This may be attributed to the improvement of roughness, porosity, wettability and topography of the surface by nanoparticle deposition.

Coatings can be classified into multilayer/monolayer and organized/unorganized structures considering the coating process. Nanoparticle deposition is usually encountered with some challenges according to the physical properties of nanoparticles. The available methods for coating with nanoparticle deposition can be distinguished through different parameters, including the ability of controlling particle density and layer thickness, the ability of using different particles, the complexity of the method as well as the required instrumentation. Various materials can be used for generating nanoparticles, such as metals, oxides of nanoparticles ceramics and polymers. The nanoparticles made of metal oxide are of great importance in chemistry, physics, mechanics and materials science. Among the applications of metal oxide nanoparticles in technology, production of microelectronic circuits, sensors, piezoelectric devices, fuel cells and anti-corrosion coatings can be mentioned. The unique physical and chemical properties of the metal oxide nanoparticles are related to the limited size and high density in corner or edge surface sites.

Stability is a significant issue in nanoparticles considering their tendency to lower their high surface energy attributed to their high surface-to-bulk ratio. Nanoparticles can reach stability through two processes: the absorption of molecules from the environments and lowering the surface area through coagulation and agglomeration [92,93]. The tendency of a nanoparticle to coagulate, which is unwanted in general, can be controlled by modifying the surface layer. In order to prevent coagulation in liquid medium, appropriate ligand molecules are generally attached to the nanoparticle surface, so that they can be solved in suitable solvents. The nanoparticle deposition on the layer leads to an improvement in the characteristics of the heated surface, including surface wettability, roughness and capillary wicking performance, which consequently results in the CHF amelioration.

Thermal conductivity of suspended nanoparticles is responsible for such amelioration in boiling heat transfer. Alumina, silica, titania and zirconia nanofluids have been widely investigated for CHF

amelioration. The use of alumina and copper nanofluids in the experimental tests of pool boiling experiments resulted in the respective CHF amelioration of 171% and 176% compared to that of pure water [94]. Correspondingly, HTC was also augmented due to the nanofluid boiling. From the investigations concerning the nanoparticle deposition on the heater surface after boiling, it was inferred that heat flux improvement can be achieved at lower concentrations. However, for the higher concentrations of alumina nanoparticles, a decrease was observed in CHF enhancement. It can be concluded that increasing nanoparticle concentration would lead to an increase in the nanoparticle deposition over the surface with a thickness of a few micrometers. This increase is followed by a reduction in the active nucleation sites. From all of these studies, it can be inferred that the use of a hydrodynamic instability hypothesis is not sufficient for justifying CHF amelioration in nanofluids. An instability hypothesis is based on water contact angle measurement, and it is a challenge to quantify the amelioration of heat transfer over thin wire surfaces [95]. From the performed observation, the insufficiency of the existing theoretical models can be concluded for the prediction of the CHF with surface effects. The basic scheme of nanoparticle layer deposition is shown in Figure 3.

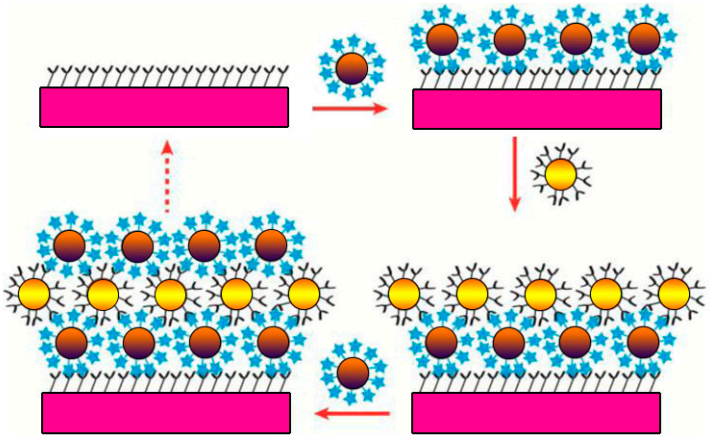

Figure 3. Illustration of the few layers nanoparticle deposition method. Reproduced from [96], Elsevier: 2016.

1.6. Objectives of the Present Review

This review paper aims to highlight the essential concepts concerning recent advances in critical heat flux amelioration of pool boiling surfaces to access the vast literature available on research methodologies. The study is concentrated on the modification of surface characteristics through the use of metal oxide nanoparticle deposition process. By reviewing the related literature, the use of metal oxide nanoparticle for CHF enhancement, nanoparticle deposition methods and the mechanism of CHF enhancement in nanoparticle deposited surfaces are analyzed. Additionally, the existing gap in the research, future works, enhancement potentials, and limitations as well as their possible industrial implementation are debated in the present review article.

2. Key Factors of Metal Oxide Nanoparticle Deposition for CHF Enhancement

2.1. Nanoparticle Material

The nanoparticle dispersion in the base fluid plays a key role in the CHF amelioration. Diverse metals, metal oxides, CNTs and diamond have been employed for pool boiling heat transfer purposes. The CHF amelioration in some pool boiling investigations is summarized in Table 1. As it can be seen, the reported CHF enhancement was different in various studies, even for the same substance. For example, despite the extensive use of alumina nanoparticles in most of the investigations, the CHF amelioration was different. In fact, the nanoparticle material, size and concentration as well as the base fluid have different impacts on CHF.

Table 1. Summary of critical heat flux (CHF) amelioration for selected pool boiling investigations.

No.	Authors	Year	Nanoparticle Material	Base Fluid	Particle Size (nm)	Concentration	Material/Type of Heater	CHF Enhancement (%)	Ref.
1	You et al.	2003	Al_2O_3	Water	-	0.001–0.025 g/L	Copper block	200	[97]
2	Vassallo et al.	2004	SiO_2	Water	15 and 20	0.5 vol.%	Ni-Cr Wire	60	[98]
3	Bang and Chang	2005	Al_2O_3	Water	-	0–4 vol.%	Plate heater	51	[99]
5	Kim et al.	2006	$TiO_2Al_2O_3$	Water	85 47	10^{-5}–0.1 vol.%	Ni-Cr heater	200 176	[100]
6	Kim et al.	2006	$Al_2O_3SiO_2ZrO_2$	Water	110–210 20–40 110–250	10^{-3}–0.1 vol.%	SS Wire	50 80 75	[101]
7	Kim et al.	2007	$Al_2O_3TiO_2$	Water	47 23	0.00001–0.1 vol.%	Ni-Cr Wire	100	[102]
8	Liu et al.	2007	CuO	Water	30	0.1–2 wt%	Copper plate with grooves	50	[103]
9	Coursey and Kim	2008	Al_2O_3	Water	45	0.001–10 g/L	Polished Copper	37	[104]
10	Golubovic et al.	2009	$Al_2O_3BiO_2$	Water	22.6–46 30	0–0.01 vol.% 0–0.01 vol.%	Ni-Cr Wire Copper	50 33	[105]
11	Kwark et al.	2010	Al_2O_3CuO	Water	139 143	0.001–1 g/L	Copper block	80	[106]
12	Huang et al.	2011	TiO_2	Water	110–220	0.01–1 wt%	Nickel tube	82.7	[107]
13	Sheikhbahai et al.	2012	Fe_3O_4	EG-Water	50	0–0.1 vol.%	Ni-Cr wire	100	[108]
14	Hegde et al.	2012	CuO	Water	10–100	0.01–0.5 vol.%	Ni-Cr wire	130	[109]
15	Kole and Dey	2012	ZnO	EG	30–50	0.5–3.75 vol.%	Copper block	117	[110]
16	Vazquez and Kumar	2013	SiO_2	Water	10	0.1–2 vol.%	Ni-Cr wire	270	[111]
17	Sharma et al.	2013	ZnO	Water	38–68	0.01 vol.%	Copper	160	[112]
18	Kim ei al.	2014	TiO_2	Water	47	0.01 vol.%	Ni-Cr wire	175	[113]
19	Naphon and Thongjing	2014	TiO_2	R141b-Ethanol	21	0.01–0.075 vol.%	Cylindrical heater	-	[114]
20	Sakashita	2015	TiO_2	Water	25	0.002 wt%	Copper	200	[115]
21	Sarafraz et al.	2016	ZrO_2	EG-Water	20–25	0.025–0.1 vol.%	Copper	-	[116]
22	Ali et al.	2017	TiO_2	Water	-	12 wt%, 15wt%	Copper block	122	[117]
23	Kshirsagar and Shrivastava	2018	Al_2O_3	Water	30	0.3–1.5 wt%	Ni-Cr wire heate	87	[118]
24	Kangude and Srivastava	2019	SiO_2	Water	-	0.005 and 0.01% (V/V)	-	-	[119]

In spite of controversies regarding the effectuality of water-based oxide nanofluids, they have recently received a considerable amount of attention. In contrast, metal nanofluids have gained less attention, which could be attributed to difficulties due to their suspension within the base fluid. Kathiravan et al. [120,121] explored the nucleate pool boiling in a water-based Cu nanofluid (0.25–1.0 wt%) and reported the highest CHF amelioration (~50%) relative to the pure water. Incorporation of 9.0 wt% SDS surfactant, however, declined the CHF amelioration to one-third. Furthermore, the nucleate boiling HTC showed a descending trend by the enhancement of nanoparticle content. Based on Zhou [122], single-phase convection was increased; the nucleate boiling heat transfer, however, was compromised with acetone-based Cu nanofluids. Krishna et al. [123] reported a reduction in the HTC of water-based Cu nanofluids (0.01 vol.%) at the low-heat-flux nucleate boiling region in comparison with the pure water. The HTC was also enhanced by raising the concentration to 0.1 vol.%. Therefore, concentration enhancement can oppositely influence at the high-heat-flux region. Such a complex trend can be assigned to various parameters such as thermal conductivity of the microlayer, sorption layer formation and active nucleation site densities. Kole and Dey [124] observed a simultaneous increase in nucleate boiling HTC and CHF by raising the Cu content (0.005–0.5 wt%) in the water-based Cu nanofluids. Moreover, they recorded higher heating rise in the copper-made surfaces compared to the brass surfaces. The nucleate boiling HTC showed an amelioration by an increase in surface roughness (R_a) from 0.06 to 0.22 μm; however, a further increase in roughness by 0.7 μm, resulted in a decline, which can be explained by deactivation of nucleation sites by nanoparticle deposition.

Shi et al. [125] explored the impact of Fe nanoparticles and observed that the nucleate boiling heat transfer depended on nanoparticles thermal properties, size and concentration, in addition to heat flux. The rise in efficient thermal conductivity of the fluid as well as the decline in surface tension at the presence of nanoparticles are associated with improved nucleate boiling heat transfer. Besides, nanoparticles' entrapment in the surface voids will further smoothen the surface and hence reduce the nucleate boiling HTC. So, they concluded that any changes in heat transfer performance are the consequence of the two mentioned factors. The boiling performance of Al_2O_3 and Cu water-based nanofluids was compared in the work of Cieslinski and Kaczmarczyk [126] on copper and stainless steel tubes. In the case of smooth copper tube, nucleate boiling HTC did not show dependence on the nanoparticle material; HTC was, however, reduced by nanoparticle concentration enhancement from 0.01 to 1.0 wt%. Besides, concerning the stainless-steel tube, nucleate boiling HTC exhibited improvement with both nanoparticle type and concentration. The substance used in heating surface seems to be ineffective on the boiling heat transfer as tested for 0.1 wt% Cu nanofluid.

The type of nanoparticles and the base fluids are demonstrated in Figure 4. Clearly, Al_2O_3, CuO and TiO_2 accounted for 33.1%, 14.5%, and 11.3%, respectively. They were followed by SiO_2 (8.2%), ZnO (6.6%), Fe_3O_4 (3.1%) and ZrO_2 (3.3%), and that 85.1% of the applied base fluid was water, in which the EG (7.7%) and refrigerants (5.2%) had the subsequent ranks. As suggested Figure 4, Al_2O_3 and CuO are the most generally utilized materials nanoparticles in water, which has the highest rate of application as the base fluid.

2.2. Nanoparticle Thermo-Physical Properties

Thermo-physical properties refer to properties with an impact on the heat transfer and storage. These properties may vary by the state variables, such as temperature, pressure and mixture components with no alternation in the chemical nature of the material. Density, thermal conductivity, heat capacity, thermal expansion, thermal radiative properties, vaporization heat, boiling point temperature, melting point, viscosity, mass and thermal diffusion coefficients, the speed of sound, surface and interfacial tension in fluids can be classified as the thermo-physical properties of a substance [127–129].

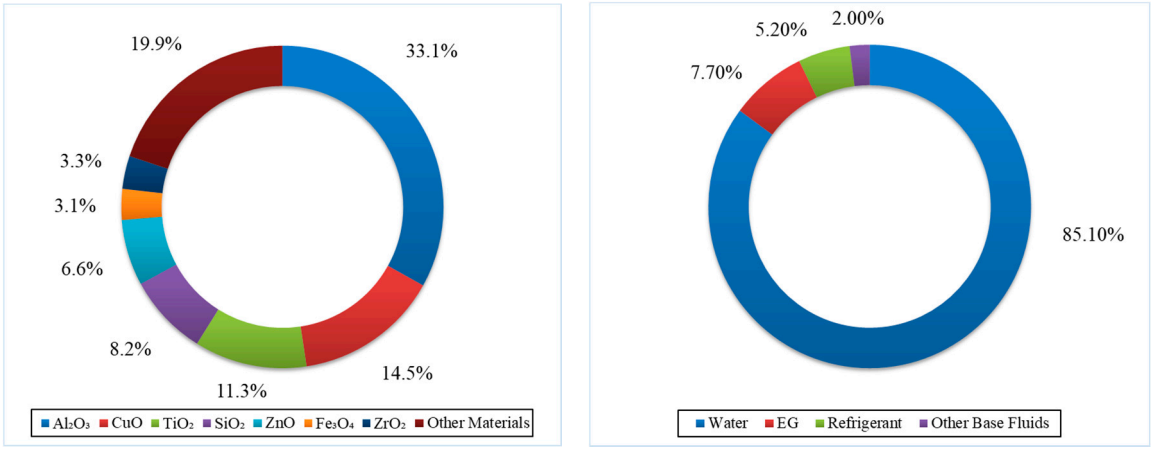

(**a**) (**b**)

Figure 4. (**a**) Materials and their percentage used as nanoparticles. (**b**) Common materials used as base fluids in the field of nanofluid pool boiling.

Numerous studies have addressed the impact of nanofluids' thermo-physical properties on their boiling performance. Nanofluid properties such as heat capacity, density and viscosity showed no sensitivity to the nanoparticles' presence; the thermal conductivity and the surface tension, however, exhibited a significant dependence on the nanoparticles. Studies have revealed that the thermal conductivity of nanofluids is greater than the conventional fluids [106,130], which can be attributed to the large specific surface area of small-sized particles, as well as an enhancement in the fluid heat capacity, Brownian motion and interfacial liquid layering [120]. As stated by Das et al. [130] and Wen and Ding [131], an augmentation in the thermal properties of a stable nanofluid can elevate its boiling heat transfer. In fact, the conduction heat transfer plays a key role in the thin fluid layer above the heating surface [132].

Lee et al. [133], Kwak and Kim [134] and Suganthi and Rajan [135] expressed the resistance of metal oxides toward oxidation which can result in their chemical stability. Moreover, some metal oxides have densities inferior to their corresponding metals which can be helpful in resolving the problem of particle settling during nanofluid formulation. This can explain the popularity of metal oxides in nanofluid formulation in spite of their inferior thermal conductivity (compared to metals). Owing to its superior thermal conductivity and low density, alumina has been widely explored for nanofluid applications.

Liu et al. [103] empirically scrutinized the nucleate boiling heat transfer in the CuO/water nanofluid at different pressures and nanoparticle contents. Their results revealed a significant impact of operation pressure on nucleate boiling profile. Furthermore, they reported an increase in the HTC and CHF of nanofluids by pressure reduction when compared to the pure water. A slow enhancement of HTC and CHF by nanoparticle content elevation (until its optimal value, 1.0 wt%) was also observed for the entire tested pressures. Beyond the optimal concentration, HTC showed a deteriorating trend, whereas CHF maintained a fixed value. This phenomenon was explored by investigating the impact of nanofluid thermo-physical properties and variations in the surface features. In the case of former parameter, nanofluid thermal conductivity, viscosity and the surface tension were considered, which showed 102%, 101% and 88% variation in comparison with the pure water, respectively. These data were then employed in the Kutateladze correlation [136]:

$$\frac{h}{\lambda}\sqrt{\frac{\sigma}{g(\rho_l-\rho_v)}} = 7\times10^{-4}Pr_l^{0.35}\times\left[\frac{q}{\rho_v h_{fg}\nu_l}\sqrt{\frac{\sigma}{g(\rho_l-\rho_v)}}\right]^{0.7}\left[\frac{P}{\sigma}\sqrt{\frac{\sigma}{g(\rho_l-\rho_v)}}\right]^{0.7} \quad (2)$$

where σ shows the liquid vapor interface tension and ρ_l and ρ_v represent the liquid and vapor densities, respectively; ν_l denotes the liquid kinematic viscosity and P stands for the pressure. Furthermore, g signifies the gravitational acceleration, λ represents the fluid thermal conductivity, h_{fg} is the latent evaporation heat and, finally, Pr_l denotes the saturated liquid Prandtl number. Variations in the fluid thermo-physical features were found responsible for the HTC degradation in nanofluid.

Concerning the latter case, it was found that as the nanoparticles' size is one or two orders of magnitude smaller than the surface roughness, their deposition will decline the surface roughness, which in turn may decline the contact leading to a reduction in boiling HTC as well as an enhancement in CHF. Besides, it was assumed that a steady porous layer is only present in the sub-atmospheric pressure. Moreover, the bubble formation under sub-atmospheric pressures is largely different from the case at atmospheric pressure. Yang and Liu [22] empirically explored the pool boiling heat transfer on a copper bar under atmospheric and sub-atmospheric pressures for the functionalized and traditional SiO_2/water nanofluids and reported a substantial difference in their boiling properties. According to them, traditional nanofluid showed an increasing trend in CHF and deteriorating pattern in HTC, whereas a slight increase was observed in the HTC of the functionalized nanofluid, while its CHF remained unchanged. In contrast to the traditional nanofluids, no nanoparticles' layer covered the heated surface during the boiling in case of a functionalized nanofluid. Such dramatic differences could be assigned to modifications in the thermo-physical properties of the functionalized nanofluid, for instance, a slight increase in its thermal conductivity, accompanied with substantial enhancement in its viscosity and a decline in its surface tension.

Fe nanoparticles were employed to formulate an EG-based nanofluid by Hong et al. [137]. According to them, Fe resulted in a higher increment in the thermal conductivity of the nanofluid when compared to Cu nanofluids.

Quan et al. [138] recently published an article on the impact of nanoparticle wettability on nucleate boiling performance. According to Figure 5, nanoparticles with moderate hydrophilicity are adsorbed to the vapor–liquid interface, preventing from liquid drainage among the adjacent bubbles. Thus, the bubble coalescence will be resisted; hence, a decline will be observed in the bubble departure diameter as well as an amelioration in the nucleate boiling HTC and CHF. Highly hydrophilic nanoparticles, however, were not adsorbed to the interface. Therefore, the bubble coalescence will remain unchanged.

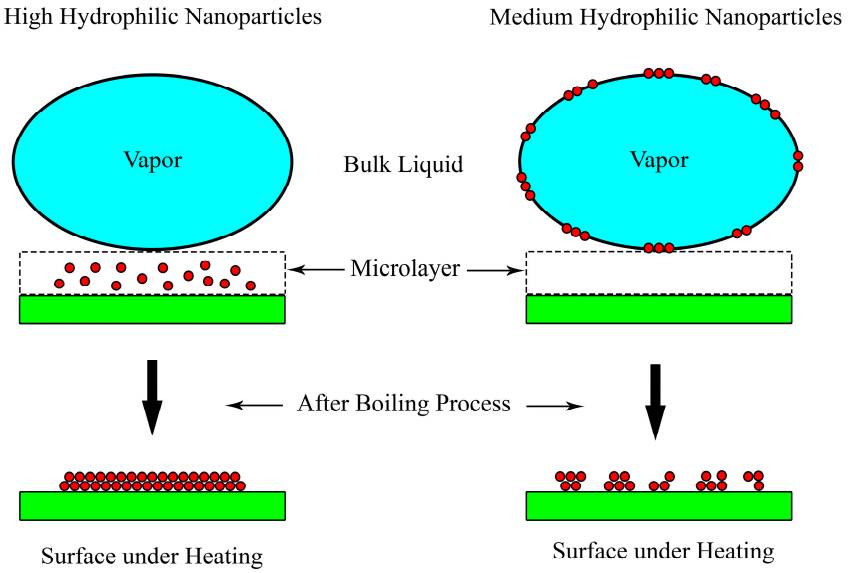

Figure 5. Illustration of nanoparticle wettability effect on deposited layer morphology. Adapted from Quan et al. Reproduced from [138], Elsevier: 2017.

As demonstrated in Figure 5, nanoparticle wettability affected the deposited layer morphology in which the high hydrophilic nanoparticle layers were relatively smooth, with uniform particle dispersion while the layers out of nanoparticles with medium hydrophilicity possessed higher roughness and irregularity.

According to Bourdon et al. [139–141], surface hydrophobicity will decline the incipience boiling superheat of water. Jo et al. [142] also tested the identical nano/microstructures (micro-patterns surrounded by nano-grass structure) with two different sorts of surface wettability (i.e., silicon-oxidized, with a contact angle of ~0°, and Teflon-coated, with contact angle of 162°), where both wettability conditions managed to significantly improve the CHF. Although the Teflon-coated sample exhibited earlier boiling incipience and larger HTC, its CHF was less than the silicon-oxidized specimen. In the work of Kim et al. [44,143], microstructural hybrid surfaces modified by nano-rods were applied. The application of these nano-rods substantially enhanced the surface wettability and liquid spreadability in such a way that the CHF improvement of the hybrid surface was equal to the sum of enhancements achievable by use of microstructures and nano-rods.

According to Sun et al. [144], oxygen vacancies in the crystal structure of TiO_2 can enhance the wettability as these vacancies tend to absorb water molecules. Such phenomenon can be observed under ultraviolet (UV) exposure, heat treatment and Ar^+ sputtering. Similarly, Takata et al. [145,146] reported a 200% improvement in the CHF of water and nucleate boiling heat transfer in the Cu-sputtered TiO_2 surface in comparison with the bare surface. Furthermore, the Leidenfrost temperature showed a significant enhancement by the decline of the contact angle. CHF improvement in water was also detected by Liaw and Dhir [147] upon wettability increment in a copper surface. They controlled the contact angle through variation in the surface oxidation degree. In contrast, Maeng et al. [148] stated that plasma sputtering induced enhanced wettability in TiO_2 on a nickel surface, which did not lead to the creation of a porous nanostructure; it also did not affect the CHF.

Kim et al. [149] recently indicated that temperature-induced wetting transitions in TiO_2 coatings can substantially influence the CHF. Their developed surface exhibited hydrophobic behavior at low wall temperatures, which altered to hydrophilic characteristics by the temperature rise. For instance, temperature increment from 100 to 200 °C caused a decline in the water contact angle from 83.1 to 32.7°. In addition to these temperature effects, a time dependency was observed in the wetting transitions [150]; thus, the boiling performance could be further enhanced by boiling time augmentation at high heat flux zones.

The thermal transport characteristics (i.e., thermal conductivity, density, specific heat, viscosity and surface tension) of the nanofluids are of crucial significance in the single-phase heat transfer purposes. Interestingly, numerous studies (with a few exceptions) have stated that these properties are not highly effective on CHF enhancement. This feature, however, should be first explored prior to examinations for the pool boiling heat transfer purposes.

The major underlying reason for incorporation of nanoparticles in the conventional fluid is the thermal conductivity enhancement. The thermal conductivity values of some common metallic and non-metallic solids as well as liquids are presented in Figure 6. Experimental or analytical methods can be applied to calculate the thermal conductivity of nanofluids. Experimental approaches such as transient hot wire [151], steady state parallel plate [152] and temperature oscillation methods [153] have been widely employed to quantify the nanofluid thermal conductivity. Among the analytical techniques for the prediction of thermal conductivity [154–157], Hamilton–Crosser [158] and Yu and Choi [159] are almost comparable while Maxwell model [160] underestimates the values with difference increase by nanofluid concentration increment [161]. Interestingly, the experimental results were far higher than the analytical outcomes reflecting the presence of a neglected heat transport mechanism in nanofluid.

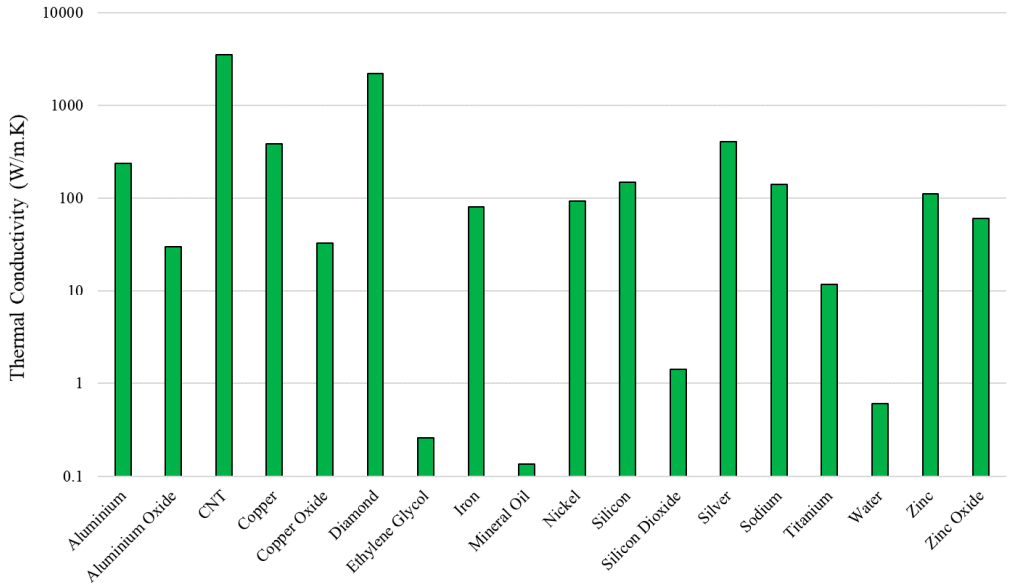

Figure 6. Comparison of thermal conductivities of metallic and non-metallic solids and liquids. Adapted from Kamatchi and Venkatachalapathy. Reproduced from [162], Elsevier: 2015.

For a deeper understanding of the nanofluid thermal conductivity and CHF improvement, You et al. [97] incorporated a very small nanoparticle content to enhance the CHF. Their employed nanoparticle concentration was substantially smaller than the practical nanoparticle content used to enhance the nanofluid thermal conductivity. Based on their observations, CHF improvement cannot be assigned to the nanofluids thermal conductivity, which was in line with the previous studies on pool boiling heat transfer [163,164]. On the other hand, Ahmed et al. [165] stated the more profound impact of nanofluids thermal conductivity compared to the rate of nanoparticles deposition at lower concentrations, which may result in CHF increment. Their observation, however, requires deeper exploration regarding the particles' size and shape, nanofluid preparation procedure as well as its stability. A recent investigation by Ahn et al. [166] indicated that a small enhancement in the thermal conductivity of reduced graphene oxide (RGO) colloids combined to surface characteristics can significantly affect the CHF delay. Yang and Liu [22] study also reported a drastic thermal conductivity increment in the functionalized silica nanofluids. Such an increment did not affect the CHF improvement, as the resulting CHF did not differ from that of pure water. Therefore, it can be inferred that the nanofluid thermal conductivity can significantly affect the CHF enhancement at lower nanoparticle contents. A comprehensive investigation on a wide spectrum of nanoparticles with various sizes is inevitable for a definite statement on CHF.

The difference in the density and specific heat values was negligible or even identical to those of pure water at the entire tested nanoparticle contents [163,167]. A comparison was made between the analytical and empirical specific heat and density of nanofluids by Pantzali et al. [168], which revealed 5% and 2% deviations in density and specific heat capacity, respectively. Therefore, nanofluids' density and specific heat can be determined by the following equations [169] in the majority of the pool boiling heat transfer studies.

$$\rho_{nf} = \rho_{bf}(1-\phi) + \rho_{nf}\phi \tag{3}$$

$$\rho_{nf}C_{Pnf} = \rho_{bf}C_{Pbf}(1-\phi) + \rho_{bf}C_{Pbf}\phi \tag{4}$$

where subscripts of nf and bf are respective expressions for nanofluid and base fluid, while ρ, ϕ and C_P denote density, concentration and specific heat capacity, respectively. In spite of a negligible variation in the analytically predicted density and specific heat values, a limited number of investigations reported a decline in specific heat by elevation of the nanoparticles content [164,170]. Regarding the

lack of a systematic study addressing the impact of density and specific heat on the CHF augmentation, a detailed investigation sounds essential to deeply explore the effect of these parameters at high nanoparticles' concentration.

The viscosity of nanofluids should be also addressed to elucidate its role in CHF improvement. The nanofluid viscosity can be determined by Brinkman equation [171].

$$\mu_{nf} = \mu_{bf}(1 + 1.25\phi) \tag{5}$$

in which subscripts of nf and bf are respective expressions for nanofluid and base fluid, while μ and ϕ denote dynamic viscosity and concentration, respectively. The mentioned equation holds for charge-free particles; it, however, underestimates the viscosity. This equation was modified by the inclusion of electro-viscous force emerged during electro stabilization [172].

$$\mu_{nf} = \mu_{bf}(1 + 10\phi) \tag{6}$$

in which subscripts of nf and bf are respective expressions for nanofluid and base fluid, while μ and ϕ denote dynamic viscosity and concentration, respectively. The nanofluid viscosity generally grows by nanoparticle concentration and declines with temperature rise, as suggested by various studies [131,173,174]. The underlying mechanisms are, however, unknown. Some studies examined the relationship between nanofluid viscosity and nanoparticle size. The viscosity can be well estimated by classical models and other formulae at lower volume fractions. The estimation, however, fails at different temperatures [175].

Concerning the impact of viscosity on CHF increment, Kwark et al. [106] evaluated the viscosity and observed a minimum difference between the viscosity of nanofluid and pure water, which could be attributed to low nanoparticle content. An incremental trend was found in the kinematic viscosity by concentration enhancement [164], which could be assigned to the electro stabilization-induced and electro viscous forces. Das et al. [130] assessed the viscosity of alumina-water nanofluid as a function of the shear rate. They recorded an ascending trend in viscosity by the growth of nanoparticles' content, while it reduced by temperature. The viscosity showed an incremental behavior by shear rate. They concluded that such patterns cannot be exploited for deteriorating the boiling heat transfer features. Currently, the viscosity values of the pool boiling studies are similar to those of pure water in all the evaluated concentrations [176,177]. Further studies are required in the following areas:

- Empirical and analytical studies to establish a database for the nanofluid viscosity.
- Application of more accurate models and/or correlations for the simulation or analysis of the nanofluid heat transfer.

The nanofluid surface tension is another key factor in CHF increase that has been extensively addressed in recent decade. Vafaei et al. [178] studied the impact of bismuth telluride (Bi_2Te_3) nanoparticle size and content on the efficient gas–liquid surface tension. Surprisingly, the surface tension declined by the enhancement of nanoparticles' content until a critical value. A further increase of nanoparticle concentration resulted in an inverse behavior. Furthermore, at similar mass concentrations, the nanofluid encompassing 10.4 nm nanoparticles exhibited higher surface tension compared to the one including 2.5 nm nanoparticles, reflecting the impact of nanoparticles size and concentration on the liquid–gas surface tension.

An empirical research on CNT nanofluids by Kumar and Milanova [179] indicated the surface tension relaxation (the difference between surface tension of nanofluid and base fluid) as the main underlying mechanism in the CHF delay. The optimization of CNT and surfactant concentrations for the heat flux maximization requires more studies. According to Kathiravan et al. [121], the incorporation of surfactant in Cu-water nanofluid will suppress the CHF increment as the result of a declined surface tension. Jeong et al. [180] also reported a decline in surface tension by Tri-sodium phosphate (TSP) and nanofluid contents' increase. Indeed, a reduction in surface tension will lower the CHF values.

The impact of nanoparticle deposition on the surface (which reduced the contact angle and hence improved the wettability) could explain the augmentation in CHF of TSP and nanofluids. Contrarily, the nanofluid surface tension remained nearly unchanged relative to pure water at all evaluated concentrations [176,177].

The surface tension generally shows a decreasing trend with a rise in nanoparticles' concentrations and temperature. The following fields should be more investigated to gain a deeper insight into the CHF enhancement: (1) synergetic influence of surface tension and surface wettability; (2) synergetic impact of nanoparticle concentrations and surfactant type.

To conclude, variations in the thermal transport characteristics do not significantly affect the CHF delay. Its role is, however, more pronounced at lower concentrations. In this regard, thermal transport parameters should be further investigated at lower volume fractions and finer particle sizes for a more reliable conclusion on the CHF enhancement.

2.3. Nanoparticle Shape and Size

The morphology of the individual particles has a significant impact on the boiling CHF and HTC. This is related to the fact that different parameters, including post-sintering pore shape, permeability, surface roughness, coating's effective conductivity and diffusivity are affected by particles morphology. The effect of particles' morphology on pool boiling has not been addressed in the literature. However, in some other applications for heat transfer, the influence of this parameter on geometrical and thermo-physical properties has been studied [181–183]. Deng et al. [184] investigated the impact of particle parameters such as shape and size on flow boiling performance of microchannels. The studied microchannel was a porous copper heat sinks being made of particles with spherical and irregular shapes (50–150 μm effective diameter). According to the obtained results, the highest HTC was observed for the irregular-shaped particles with smaller sizes (50–75 μm). However, for the spherical-shaped particles with smaller sizes, the lowest HTC was achieved.

It can be inferred that the nanoparticle size plays a significant role in the amelioration of pool boiling CHF [185]. As the size of nanoparticles increase, better boiling heat transfer performance would be achieved for the nanofluids [186,187].

The effect of nanoparticle concentration in the base fluid was investigated by Kole et al. [110]. Two diverse concentrations of ZnO nanoparticles with a size of 30–40 nm in ethylene glycol base fluid were evaluated. It was observed that, after pool boiling, nanoparticles were deposited over the heater surface, which prevented the active nucleation sites, and, therefore, HTC decreased. By measuring the CHF values through the use of thin Constantan wire, they observed the significant increase in CHF by increasing the concentration of ZnO. They reported a maximum CHF enhancement of 117% for ZnO nanoparticle volume fractions of 2.6%. Moreover, they inferred that the CHF amelioration is associated with the increased surface roughness of the heating wire as a result of nanoparticle deposition.

Peng et al. [188] performed an empirical study on the impact of Cu nanoparticle dimensions on nucleate pool boiling heat transfer of R113/oil mixture. According to the obtained results, the maximum increase of 23.8% was achieved for HTC by reducing the nanoparticle dimension from 80 to 20 nm. Additionally, smaller Cu nanoparticles would lead to a higher nucleate pool boiling HTC.

An empirical analysis of nanoparticle size impact on pool boiling was conducted in some studies [189,190]. However, satisfactory evidence and validation were not provided for the obtained results. The influence of size and concentration of the nanoparticle on the boiling performance was investigated by Hu et al. [191] for SiO_2 nanofluid. They reported the increasing trend of HTC by decreasing the nanoparticle size from 120 to 84 nm.

2.4. Nanoparticle Concentration

The impact of diverse concentrations of Al_2O_3/water nanofluids on the pool boiling of a smooth horizontal flat surface was studied by Bang and Chang [99]. According to the obtained results, as the concentration of the nanoparticles increased, worse heat transfer performance was observed compared

to pure water. However, the CHF enhancements for horizontal and vertical pool boiling were reported to be 32% and 13%, respectively.

In an experimental investigation by Golubovic et al. [105], the effect of the concentration, size and type of nanoparticles on CHF was evaluated under saturated conditions. The Al_2O_3-BiO_2/water nanofluids were used on a Ni-Cr wire, which was submerged in a chamber with dimensions of $70 \times 70 \times 100$ mm. Based on Figure 7 CHF enhances by the particle concentration increment. However, after reaching the maximum heat flux, a further increase in the particle concentration does not show any significant impact on CHF. The maximum CHF enhancements were 50% and 33% for alumina and bismuth oxide nanofluids, respectively.

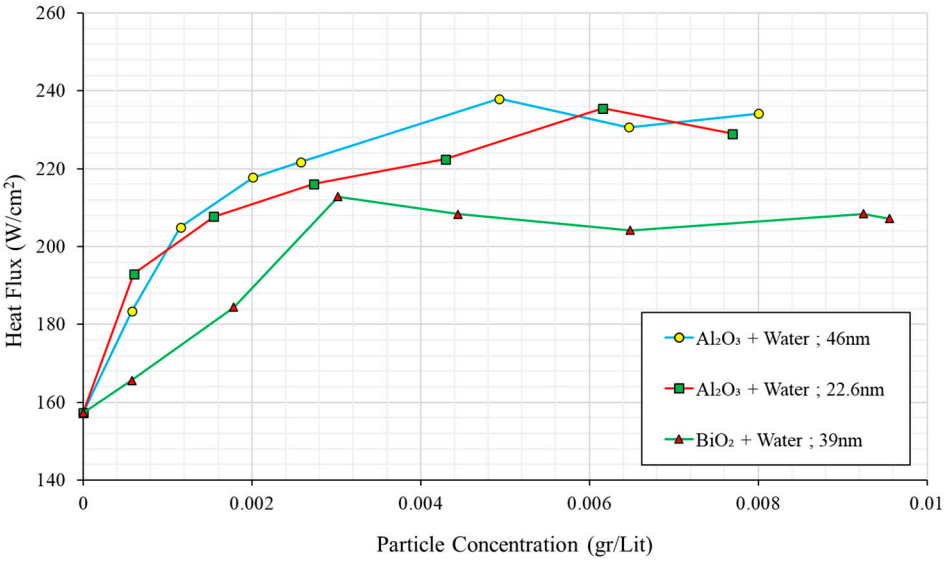

Figure 7. CHF evaluation under variations of particle concentration, material and size. Reproduced from [105], Elsevier: 2009.

The CHF performance of TiO_2-Al_2O_3-SiO_2/water nanofluids was investigated by Kim and Kim [192] by the use of Ni-Cr wire with diameter of 0.2 mm. As can be seen in Figure 8, they reported CHF enhancement by the use of nanofluids. Besides, they declared the strong dependency of CHF on the nanoparticle type and concentration.

The effect of different nanofluids, including alumina, titania and magnetite nanofluids on improving the CHF was explored by Lee et al. [193]. The experiments were conducted in saturated conditions and under atmospheric pressure by the use of Ni-Cr wire, which was embedded in a rectangular stainless-steel vessel with the dimensions of $250 \times 100 \times 230$ mm. Regarding the results, they reported the maximum CHF by concentration increment for the magnetite-water nanofluid. They justified the CHF increase by the increased surface wettability as a result of a higher frequency of departing bubbles in magnetite-water nanofluid (MWNF).

In an experimental study, Jung et al. [194] evaluated the effect of a stabilizer on CHF and boiling HTC. The considered nanofluid was Al_2O_3/water nanofluids, which was studied upon a plate Cu heater in the rectangular test chamber (1650 mL). In addition, polyvinyl alcohol (PVA) was utilized as a steric stabilizer. They stated the lower boiling HTC despite the higher CHF of nanofluids compared to the base fluid by increasing the nanoparticle concentration. Moreover, they declared that up to a critical concentration of nanoparticle (10^{-3} vol.% in this investigation), a higher effective boiling surface area was formed by the use of a stabilizer. However, further increase in the concentration would lead to a reduction in the effective boiling surface area. They found that the effective boiling surface area was increased by the deposition of the nanoparticles, which would result in the CHF amelioration, consequently.

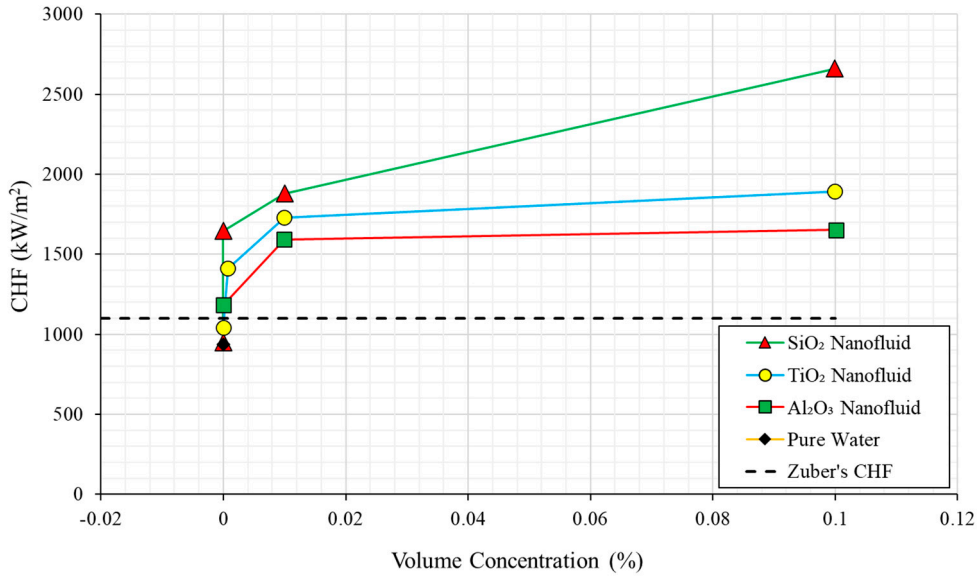

Figure 8. Variations of CHF against volume concentration for pure water and diverse nanofluids. Adapted from Ciloglu and Bolukbasi. Reproduced from [77], Elsevier: 2015.

In another study by Shahmoradi et al. [74], an increase in the surface roughness was reported by the increase in nanoparticle concentration as a result of higher particle size compared to the surface roughness (as can be seen in atomic force microscopy (AFM) images in Figure 9). Besides, the CHF enhancement was obtained according to the improved wettability.

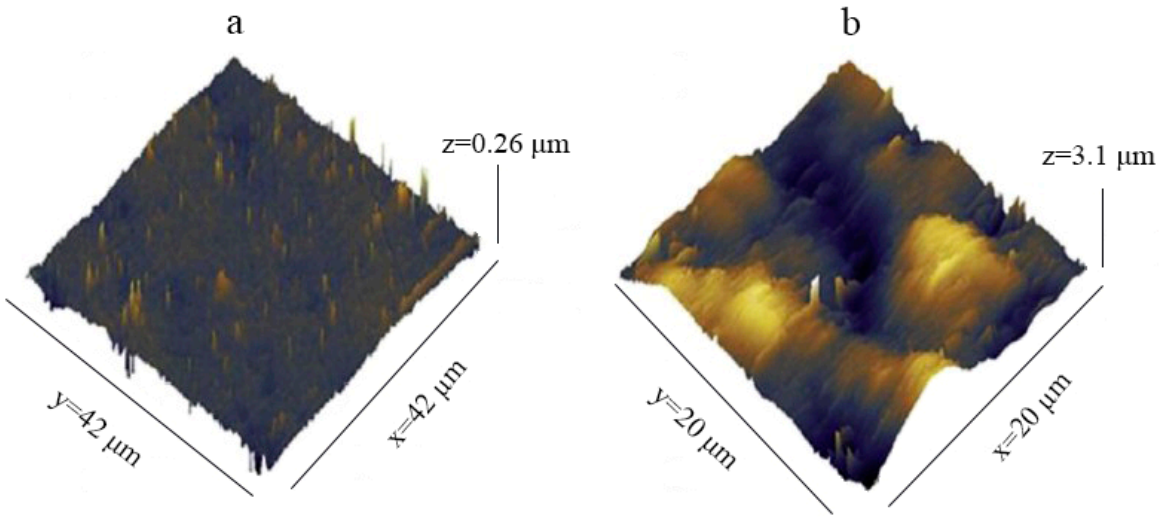

Figure 9. AFM images for (**a**) polished surface prior to boiling Ra = 5.1 nm and (**b**) surface after boiling 0.02 vol.% nanofluid, Ra = 376 nm. Adapted from Ciloglu and Bolukbasi. Reproduced from [77], Elsevier: 2015.

As was obvious from Figure 10, a significant impact of nanofluid concentration on CHF augmentation was reported by You et al. [97]. In this figure, it can be observed that the CHF values for nanofluids are almost three times the corresponding value for water at a lower saturation temperature of $T_{sat} = 60\ ^{\circ}C$ (Al_2O_3). In addition, intensive CHF amelioration was observed by increasing the nanoparticle concentration at low concentrations, which becomes almost constant at concentrations higher than 0.01 g/L. A similar trend was observed in several investigations [101,103,192,195]. In the study by Yang and Liu [22], no amelioration in CHF was reported by increasing the concentration of

functionalized silica nanoparticles [21] from 0.5 to 2.5 wt%. This was justified by the grafting silanes to the surface of silica nanoparticles.

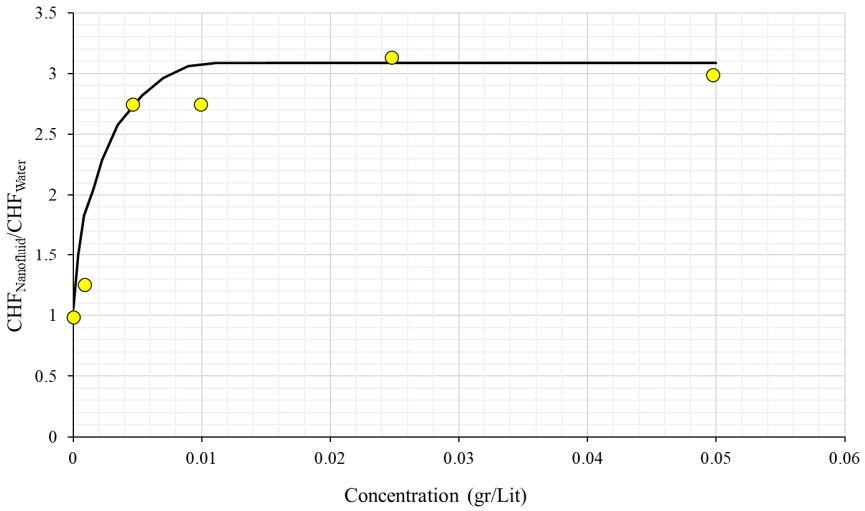

(**a**)

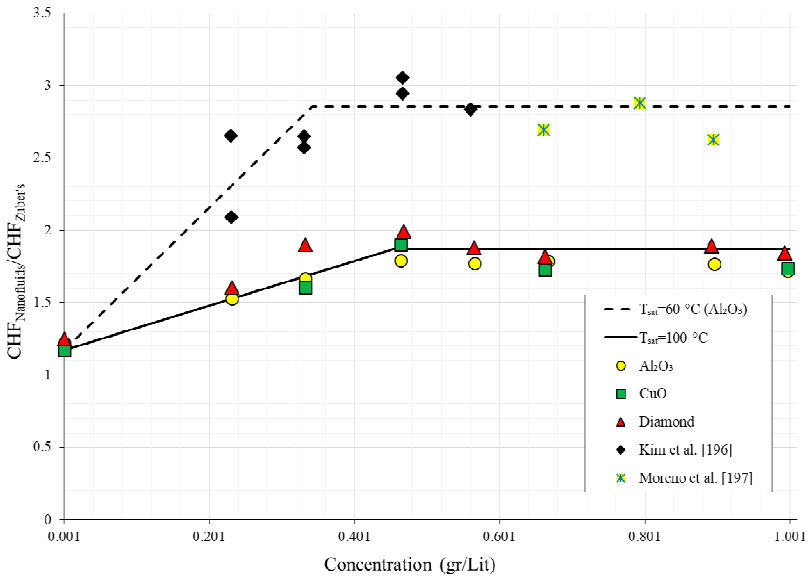

(**b**)

Figure 10. Influence of nanofluid concentration on CHF amelioration (**a**) from You et al. [97] and (**b**) from Kwark et al. [106] compared to [196,197]. Adapted from Mori and Utaka. Reproduced from [68], Elsevier: 2017.

The impact of utilizing Al_2O_3 as nanofluid for improving the pool boiling features of a copper surface with the average roughness of 177.5 nm–292.8 nm was studied by Ham et al. [198]. The alumina nanoparticles with the concentrations of 0, 10^{-3}, 10^{-2}, 0.05, and 0.1 vol.% were added to the water (as the base fluid). It was observed that CHF was increased up to 224.8% and 138.5%, respectively. When the increase in the concentration of nanoparticles reached 0.1 vol.%, a reduction was observed in the CHF behavior. This behavior is related to the variation in surface roughness. Regarding these findings, the significant impact of surface roughness, as well as nanoparticle concentration in heat

transfer properties, can be inferred. The effect of diverse nanoparticle concentrations in CHF behavior for [95,199,200] is depicted in Figure 11.

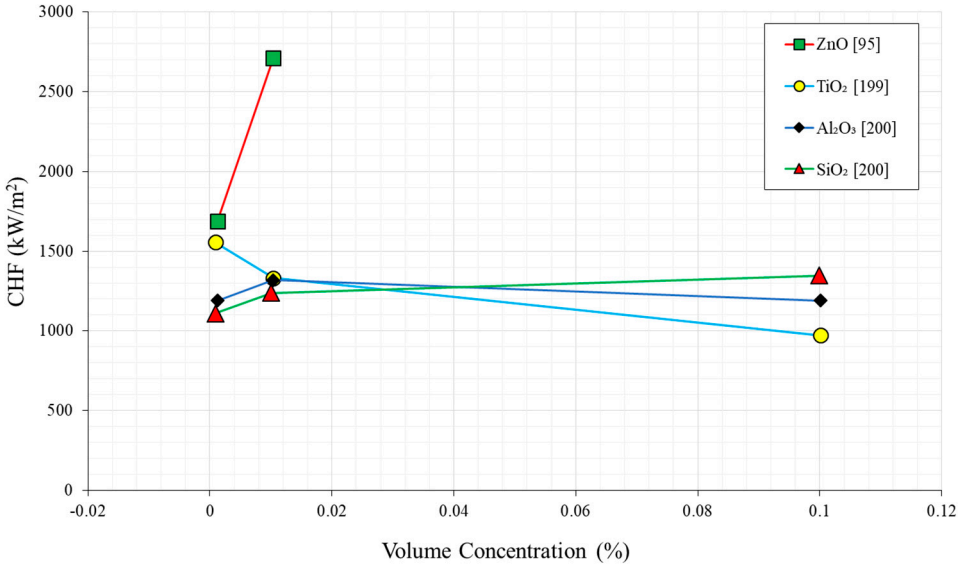

Figure 11. Variations of CHF against volume concentration for diverse nanofluids. Adapted from Prakash and Prasanth. Reproduced from [201], Elsevier: 2018.

Sarafraz et al. [116] studied the impact of different concentrations of Zirconium oxide nanofluids in a water–ethylene glycol (50:50) mixture on heat transfer behavior. Four volumetric concentrations of 0.025%, 0.05%, 0.075% and 0.1% were considered for the mentioned nanofluid. It was observed that the CHF was increased up to 29% according to the particle deposition over the heater surface, which tincreases the roughness and wettability. Moreover, the contact angle was changed from 86.2° to 58.2° by increasing the volumetric concentration of nanoparticles. The ameliorated heat transfer was attributed to the capillary wicking into the porous layer, which affects the dry-spot rewetting considerably.

The heat transfer features of water-based nanofluids were scrutinized by Sulaiman et al. [202] through performing pool boiling experiments. Both material and concentration were considered in this study. The working fluid was obtained by the addition of TiO_2, Al_2O_3 and SiO_2 with the respective mass concentrations of 0.04, 0.4 and 1 kg/m^3 in water. It was observed that both parameters of material and concentration play important roles in increasing the CHF. In higher concentrations, almost 2.5–3 times CHF enhancement was observed compared to the CHF of water.

CHF enhancement by the utilization of TiO_2 nanoparticles was studied in many studies [94,200,203–205]. In Figure 12, the TEM image of TiO_2 nanoparticle dispersed in water can be seen. For the nanoparticle concentration equal to 0.001 vol. %, the maximum CHF amelioration equal to 30% was observed. A further increase in concentration was followed by a slow decrease in CHF [206]. This trend can be justified by the fact that increasing the nanoparticle concentration suppresses the distribution of active nucleation sites, which results in lesser dry spot rewetting.

Hiswankar and Kshirsagar [199] performed a study for evaluating the effect of nanoparticle concentration on CHF behavior. It was found that, for smaller nanoparticle concentrations, CHF was improved up to 170%. This amelioration was because of the increase in the surface roughness as a result of nanoparticle deposition on the heater surface. Therefore, it can be concluded that a trade-off should be performed between different parameters, such as nanoparticle concentration, surface roughness and a reduction in nucleation sites. For this purpose, an optimization can be conducted on the size of nanoparticle.

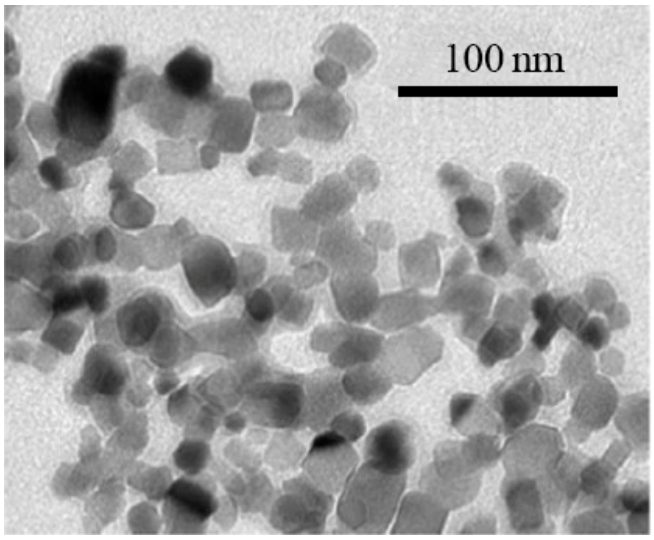

Figure 12. TEM demonstration of titanium oxide in water. Reproduced from [201], Elsevier: 2018.

According to the results of [207], 80% CHF amelioration can be achieved by the dispersion of 0.001 wt% ZnO nanoparticle in the water. However, the CHF performance deteriorates in higher concentrations due to the deposition of a thick layer of nanoparticle deposition on the heater surface. This investigation introduced a preliminary idea for the selection of the type and concentration of nanoparticles in the working fluid.

An empirical study on the impacts of different parameters of nanofluids was performed by Ciloglu and Bolukbasi [77] for pool boiling CHF. They declared the significant effect of nanoparticle concentration on CHF behavior. In addition, they found that the maximum CHF amelioration occurred in an optimum value of nanoparticle concentrations. Before this optimum value, increasing the concentration would lead to an increase in CHF, while, after this point, CHF remains constant by a further increase in concentration. In the investigation of Kole and Dey [124] for the water-based Cu nanofluids, it was found that the CHF increases by raising the concentration of nanoparticle in the range of 0.005–0.5 wt%.

Sarafraz et al. [116] scrutinized the ethylene glycol/water-based with 0.025–0.1 vol.% ZrO_2 nanofluids and 50 vol.% glycol, experimentally. They also confirmed the increasing trend of CHF with increasing the nanoparticle concentration. The boiling performance of H_2O/LiBr-based binary Al_2O_3 nanofluids was studied by Jung et al. [208]. They used polyvinyl alcohol as a stabilizer and reported the CHF amelioration by increasing Al_2O_3 concentration from 0.01 to 0.1 vol.%. Moreover, Lotfi and Shafii [209] reported CHF reduction for 0.5–4 wt% Ag and 0.125–1.0 wt% TiO_2 nanofluids as the nanoparticle concentration decreases. The boiling properties of a honeycomb porous plate, which covers a 30-mm diameter heating surface that was placed in water-based TiO_2 nanofluids was studied by Mori et al. [210,211]. They achieved considerable CHF amelioration equal to 320 W/cm^2 by increasing the nanoparticle concentration to 0.1 vol.%.

2.5. Nanoparticle Dispersion Method

The method for the dispersion of a nanoparticle into the base fluid is of great significance as it affects the characteristic as well as the agglomeration of nanoparticles [192,212,213]. By reviewing the available studies, it was found that the existing experimental data were different even for the same nanoparticle material, which may be attributed to the different dispersion methods of the nanoparticles in the base fluids [77,137].

Nanofluids can be prepared using either two-step or one-step processes [161,214]. In the prior method, nanoparticles, nanotubes, or nanofibers are formed as dry powder through the physical or chemical treatments such as condensation of inert gas and deposition of chemical vapor in the first step.

In the subsequent step, the powder is dispersed into the base liquid. Aggregation of nanoparticles in the fluid is considered as an important challenge in two-step processes. Moreover, inefficiency of the two-step process in dealing with heavier metal nanoparticles despite the fairly good performance for oxide nanoparticles can be considered as the other challenge. In the one-step process, the synthesis and dispersion of nanoparticles into the base fluid are conducted at the same time. However, even though this process provides superior dispersibility and stability in comparison with the two-step processes, the complexity of the process due to the stringent preparation requirements is regarded as the challenge. It should be noted that most of the conducted studies concerning nanofluid pool boiling were performed using two-step methods.

Nanofluid preparation is an important factor. Particle deposition and high thermal resistance can be generated as a result of improper preparation. Stability and appropriate distribution are considered as the effective parameters for preparing nanofluids. The appropriate preparation can be obtained through the use of the following processes [215]:

- Changing the pH of the solution via the addition of acid to keep the nanoparticles away from their isoelectric point;
- The addition of surfactants and/or dispersants;
- Stabilization through the use of ultrasonic vibration or electrostatic stabilization.

Based on the performed studies, the rheological behavior of the fluid and the nucleate boiling heat transfer can be affected by the first and second processes [131,216,217]. Pool boiling heat transfer of the aqueous-based alumina nanofluids with adjustable pH solution was conducted by Wen and Ding [131], experimentally. In order to improve the CHF performance, solvable additives such as TSP, sodium lauryl sulfate (SLS), and sodium lauryl benzene sulphonate (SLBS) were utilized in most of the studies in the field of pool boiling heat transfer [218,219]. In an empirical investigation by Jeong and Kwon [220], the impact of ultrasonic vibration on CHF was examined under natural convection condition. The CHF measurements were conducted in the presence and absence of ultrasonic vibration applied to the distilled water as the working fluid. Regarding the obtained results, it was found that applying the ultrasonic wave to water results in the CHF improvement. As visual observation showed, it can be inferred that there is a close relation between the CHF amelioration and dynamic behavior of bubble generation and departure in the acoustic field.

3. Key Surface Factors of Deposited Nanoparticle for CHF Enhancement

The processes by which the nanoparticles are attached to the solid surfaces that are called substrates and the resultant coatings of nanoparticles are formed are referred to as nanoparticle deposition. Different structures of coatings, including monolayer/multilayer and organized/unorganized structures, would be achieved due to the used coating method. Several coating methods have been proposed for nanoparticle deposition. The difference of these methods is in their capability of controlling the density and layer thickness of particle packing, their ability to use different particles, the complexity of the method as well as the required instrumentation [221–223]. As mentioned in the previous sections, the use of nanofluid in pool boiling heat transfer would lead to CHF amelioration as a result of nanoparticle deposition on the heating surface. Recently, different heating surfaces were utilized in the boiling heat transfer. The empirical results of flat plates and thin wires were reviewed by Kim [224]. It was inferred that flat plates are more reliable; however, thin wires would lead to the better amelioration of CHF.

It is worth understanding the mechanism of nanoparticle deposition on the heating surface. Microlayer evaporation was considered as the reason behind nanoparticles' deposition on the heater surface by Kim et al. [102]. They declared that the formation of a microlayer at the base of the bubbles is generally because of the nanoparticles left behind the evaporating liquid. Therefore, nanoparticles are bonded to the heater surface as a result of microlayer evaporation.

In another study by Kim et al. [100], it was reported that the growth of the deposited layer was attributed to the natural convection or gravitational sedimentation. Additionally, they stated that the CHF amelioration of nanofluids was due to the deposited layer. Moreover, Bang and Chang [99] introduced the particles deposition (not increased concentration) as the responsible factor for CHF amelioration. For a better understanding of the deposited layer effect, two sets of experiments were performed by Kim and Kim [203]. The first test was conducted with nanofluid and bare heater wire, while the second one was performed with nanoparticle-deposited wire and pure water. According to the obtained empirical data, they concluded that the CHF value in the second experiment was 1.35 times greater than the corresponding value in the first experiments. These results were consistent with the result of Kwark et al. [106]. In the latter study, they confirmed the good bonding strength of the deposited layer even after 16 consecutive experiments, which emphasizes the great role of nanoparticle deposition on CHF enhancement. Moreover, it was found that not only the nanoparticles were deposited but also solvable salts may be deposited during the boiling of nanofluids, which may be responsible for the CHF amelioration [225].

Surprisingly, in the boiling of functionalized silica nanofluids, no deposited layer was formed in all concentrations and pressure ranges. This was followed by an insignificant CHF variation [22]. In a recent research by Kim et al. [100], two key parameters were stated to be influential in the physical mechanism of CHF amelioration for deposited wire. The thickness of porous structure and capillarity phenomena; the former is responsible for holding the additional liquid microlayer, while the latter supplies the liquid toward dry area underneath growing bubbles. In the following section, the surface roughness, surface wettability and capillary wicking structure that are considered to play key roles for the CHF enhancement are discussed.

3.1. Surface Roughness

As a result of increasing the concentration of nanofluids, the deposited layer grows on the heater surface. On the other hand, a direct relationship is established between the surface roughness and deposited layer, which has been confirmed in several studies [113,226]. For example, for alumina-water nanofluid, the surface roughness of 0.5 vol.% was lower than that of 0.01 vol.%. This could be due to the lesser uniformity of the deposited layer on the surface, which would lead to the higher heat transfer rates compared to the boiling pure water with nanoparticle deposited surfaces [165].

For a better understanding of the surface roughness effects, rough and smooth surfaces were studied experimentally by Wen et al. [227]. According to the obtained results, particle deposition on the heating surface would result in the increased roughness on the smooth surface. However, no significant variation was illustrated for the rough surface. Moreover, they claimed that the surface modification was performed by the inherent feature nanoparticles every time after boiling. In contrast, for rough surfaces, the arithmetic surface roughness was increased by increasing wall superheat. The inverse trend was observed for the smooth surfaces [164]. In fact, surface roughness is a dominant factor over the surface wettability. Furthermore, the boiling heat transfer of nanofluids was about 2 times that of the base fluid for the rough surface. For the smooth surface, approximately a 30% reduction was observed when boiling with nanofluid in comparison with base fluid.

Although the average surface roughness reduced from 0.167 to 0.099 μm after boiling experiments, the CHF amelioration was accomplished. This can be attributed to the changes in surface microstructure and improved topography [121]. Utilizing ionic additive (nitric acid) is an alternative way, which affects the formation of self-assembled nanoparticle structures on the heater surfaces. In this way, a more uniform and smoother structure would be formed, which reduces the CHF enhancement [228].

It can be stated that, based on the particle deposition, the surface roughness of the heating surface was not constant. Furthermore, CHF was reduced as the result of thermal insulation caused by the continuous growth of the deposited layer. In order to obtain the optimum value for the thickness of deposited layer, which corresponds on the maximum CHF, supplementary investigations are required.

It was also inferred that the boiling performance of nanofluids was affected considerably by the transient nature of nanofluid.

3.2. Surface Wettability

The surface wettability amelioration is one of the prominent parameters in the pool boiling heat transfer of nanofluids [229]. Based on Kolev's model [230], variations of contact angle significantly affect the CHF. Accordingly, Figure 13 presents a decrease in contact angle from $\pi/2$ to $\pi/8$ giving rise to a 2-fold CHF increment. In the mentioned figure, $\theta = \pi/2$ was regarded as a reference on which all other cases were normalized. Not only static contact angle, but dynamic contact angle also have an effect on bubble dynamic and pool boiling performance [231]. The empirical findings of Kim et al. [102] were consistent with the impact of contact angle for all the evaluated nanofluids, including alumina, zirconia and SiO_2. Furthermore, surface wettability and contact angle are inversely correlated [146]. The influence of the surface tension and contact angle of TSP and nanofluids has been addressed by Jeong et al. [180]. Accordingly, a decline in the contact angle managed to ameliorate the surface wettability, and hence led to CHF amelioration in both fluids. These results are in line with other investigations in the field of pool boiling [100,104,108,192].

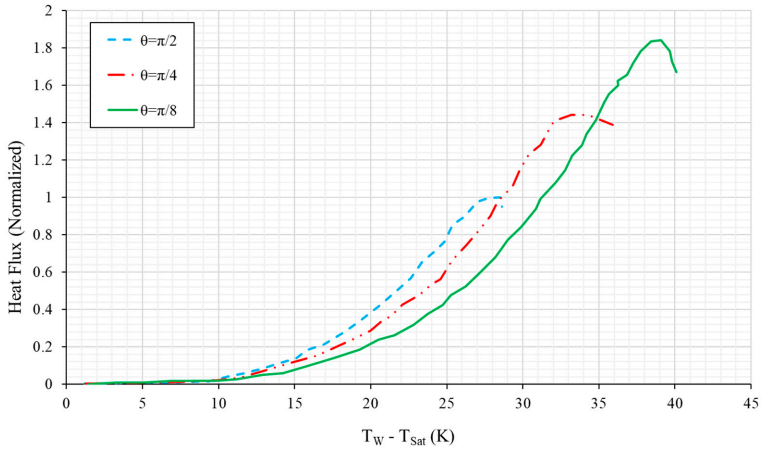

Figure 13. Variations of normalized heat flux versus wall superheat temperature at diverse contact angles. Adapted from Kamatchi and Venkatachalapathy. Reproduced from [162], Elsevier: 2015.

Figure 14 illustrates the contact angle variations in distilled water and alumina-water nanofluid. The decrease in contact angle can be attributed to the nanoparticles residing on the heater surface. The wettability can also alter the nanoparticle content of the base fluid in a way that the concentration of alumina-water nanofluid experienced a 2-fold amelioration by the contact angle decline from 46.5° to 33° [105,232].

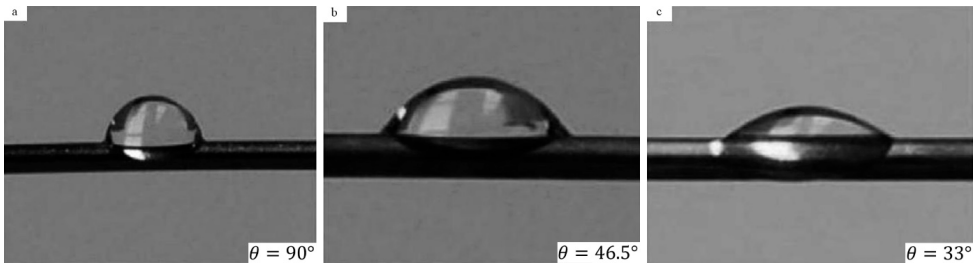

Figure 14. Contact angle determination: (**a**) water droplet over the heater surface; (**b**) droplet of Al_2O_3-water nanofluid (2.57 mg/L) over the heater surface deposited by nanoparticles after the boiling process; (**c**) droplet of Al_2O_3-water nanofluid (0.00646 g/L) over the heater surface deposited by nanoparticles after the boiling process. Reproduced from [105,232], Elsevier: 2009.

The influence of surface wettability was also addressed by Park et al. [233] in alumina-water and graphene/graphene oxide nanofluids, where no definite surface wettability–CHF amelioration relationship was observed. Moreover, they found that the variation of CHF amelioration-corresponding wavelength was more profound than the impact of contact angle in all studied nanofluids. A recent study by Ahn et al. [234] indicated that the wettability alone fails to completely justify the CHF amelioration upon the use of graphene oxide (RGO) colloids. Additionally, they concluded the CHF amelioration can be assigned to the synergetic impacts of surface wettability and the contact angle dynamics during water absorption as well as the liquid-saturated porous environment as the consequence of water absorption onto the base graphene multilayer and the self-assembled inter-connected graphene layer.

3.3. Capillary Wicking

The impact of surface wettability cannot sufficiently describe the further enhancement of CHF beyond the attainable values in cases where the contact angle is close to zero (reported by Kim et al. [100]). Moreover, the liquid rise on the capillary-induced deposited nanoparticles can be determined by:

$$L_c = \frac{2\sigma cos\theta}{R_c \rho g} \tag{7}$$

in which σ, θ, R_c, ρ and g are liquid vapor interface tension, contact angle, density and gravitational acceleration, respectively. The phenomenon of capillary wicking on the nano-porous layers will delay the dry-out and cool the dried spots giving rise to an ameliorated CHF [204]. The retarded CHF is not only attributed to the ameliorated surface wettability but also the capillary impacts originated from the nanoparticle deposition. Consideration of capillarity cannot completely elucidate the CHF enhancement for grapheme/grapheme-oxide nanofluids [233] as other factors, such as wavelength modulation during the nanofluid boiling are also involved. The influence of water absorption phenomenon was addressed by Ahn et al. for the saturated porous layers during the RGO nucleate boiling [235]. The substantial CHF amelioration (320%) cannot be fully justified considering the capillary wicking solely. In a recent investigation by Kim et al. [100], the capillary rise of all nanoparticle deposited wires was explored, where the CHF value exhibited a strong dependence on the water rise on the fouled heater wires, although all the deposited wires possessed the same contact angles. Capillarity trend showed an initial increment by the thickness of the deposited nanoparticle layer, which can be attributed to the larger number of micro-scaled structures. Further augmentation of the nanoparticles layer thickness resulted in no capillarity elevation since the valleys were already filled by the nanoparticles.

According to the available literature, the capillary wicking during the boiling of nanofluids can significantly affect the CHF enhancement. The capillary rise alone, however, does not suffice to completely elucidate the underlying mechanism of CHF improvement in the majority of the studies. The general census of the phase change heat transfer community recognizes the nanoparticle deposition as the most influential factor in the CHF amelioration. The impact of nanoparticle-induced surface modifications should be deeper studied by investigating the combined influences of surface roughness and wettability (contact angle) along with the capillary wicking. These results can be helpful in clarifying the CHF enhancement mechanism for a wide range of nanofluid contents with various particle sizes.

4. Mechanisms of CHF Enhancement

Possible mechanisms of CHF amelioration upon nanoparticle deposition on the surfaces are discussed in this section. Despite the many types of research during the last century on CHF phenomena, the establishment of a robust general correlation between empirical results and the physical process underlying the CHF amelioration has remained elusive. As discussed in the previous section, nanoparticle deposition can change the surface properties and it has an effect on CHF. Five different mechanisms have been introduced to connect the surface properties on CHF prediction: hydrodynamic instability [236], macrolayer dry-out [237], bubble interference [238], hot/dry spot [239]

and interfacial lift-off [240], among which, the theory of hydrodynamic instability by Zuber [236] has gained the highest popularity as the first theoretical and mechanistic modeling for CHF. Most of subsequent pool boiling CHF studies tried to enhance the predictive ability of Zuber's model by considering the parametric impacts neglected in the original model.

4.1. Hydrodynamic Instability Model

Based on Zuber [241], the hydrodynamic instability model is based on the assumption that the latency in CHF is highly dependent on the hydrodynamics of the vapor and liquid countercurrent flows at a relatively large distance from the top of the heated surface. This theory expresses that an ameliorated superficial vapor velocity will result in an upward movement of the vapor, which will inhibit the downward flow of liquid to the heater surface for increased heat fluxes. Such a condition will lead to an instability, which finally will give rise to CHF. The superficial vapor velocity (j_v) causing the instability above the flat upward-facing heated surface was determined by Zuber as:

$$j_v = 0.131 \left[\frac{\sigma(\rho_l - \rho_v)g}{\rho_v^2} \right]^{\frac{1}{4}} \tag{8}$$

where the subscripts of l and v are respective expressions for liquid and vapor, while σ, ρ and g denote liquid vapor interface tension, density and gravitational acceleration, respectively. Thus, the CHF of a saturated boiling can be presented by:

$$q_{CHF,Z} = j_v \, \rho_v \, h_{fg} \tag{9}$$

where h_{fg} represents the latent heat of evaporation. Many studies have confirmed the validity of the hydrodynamic instability model to elaborate the CHF amelioration mechanism in a nanofluid. For example, the study by Kim et al. [102] can be mentioned, which used the hydrodynamic model as an interpretative tool for CHF amelioration in nanofluids since its stability could consider the surface impacts including wettability and roughness. Moreover, an earlier study by You et al. [97] declared that some key but unknown factors missing in Zuber's theory were responsible for CHF amelioration in nanofluids. For CHF enhancement interpretation in nanofluids, Zuber's theory was further modified by Lienhard and Dhir [242], who included the size and geometrical impacts. They also theorized that the variations in the surface contact angle can alter the size and spacing of the vapor jets located above the heater surface. The hydrodynamic theory is recently widely questioned, even in the case of pure fluids [243].

4.2. Macrolayer Dry-Out Model

Developed by Haramura and Katto, the macrolayer dry-out model [237] considers large mushroom-shaped bubbles above the heated surface for a sufficiently long time prior to their departure. Based on this model, CHF occurs at an adequately high heat flux for the macrolayer evaporation before the mushroom bubble departure. Kim et al. [102] showed that the macro-layer dry-out theory indicates a strong correlation between CHF amelioration and the surface wettability augmentation due to nanoparticle deposition. Calculating the macrolayer thickness by the Sadasivan model [244], they detected a decline in contact angle from 70° to 20°, which could be attributed to nanoparticle deposition giving rise to a four-fold elevation of the liquid layer thickness and hence a 400% increment in CHF. The dent-like structures of the porous layers of TiO_2 on wires were also addressed [100]. This layer is capable of holding liquid and increasing the efficient liquid layer thickness in the macrolayer model for CHF. A limit was, however, indicated in CHF regardless of the liquid rise and/or TiO_2-deposited wires' thickness; it requires deeper investigations to elucidate the underlying mechanism.

4.3. Bubble Interaction Model

Rohsenow and Griffith [238] suggested bubble interaction theory for the heated surface, which postulates the occurrence of CHF, particularly at high wall superheats. The number of bubbles and the departure frequency become very high, meaning that the bubbles coalesce radially. This prevents the liquid flow towards the surface. The impact of shear force created by the mutual interactions of the growing and departing bubbles is contained in most of the developed models. The bubble growth cycle was cut prematurely by shear force, resulting in a decrease in bubble departure diameter, leading to lower latent heat removal upon departure. Based on Kolev model [230], the heat flux in the nucleate boiling region and the wall superheat can be stated as:

$$q \propto \frac{n^{\frac{1}{4}}\left(\mathrm{T_w} - \mathrm{T}_{sat}\right)^2}{\left(1 + 0.3\frac{\Delta\tau_w}{\Delta\tau_d}\right)^{\frac{1}{2}}} \tag{10}$$

where subscripts of w, sat and d are respective expressions for wall, saturation and departure, while n and T stand for active nucleation site density and temperature, respectively. Furthermore, the nucleation site density will reduce by contact angle, as observed by Wang and Dhir [245]. Therefore, the shear stress intensity due to the mutual interaction of bubbles will have a slower growth on a low-contact angle heated surface compared to the one having a larger contact angle. According to Kim et al. [102], the bubble interaction theory accounts for surface wettability amelioration as a probable mechanism of CHF amelioration.

4.4. Hot/Dry Spot Model

4.4.1. Yagov Model

The hot/dry spot procedure associates CHF to abundant small dry spots located on the heater surface during nucleate boiling. The mentioned model was first developed by Yagov [246] in 1988 and then amended by Yagov [239] in 2014. Some studies tried to extrapolate CHF from nucleate boiling models [247–250]. According to Van Ouwerkerk [251], the initiation mechanism of CHF based on the hot/dry spot model can be regarded as an irreversible growth of the dry spot area on a surface (see Figure 15).

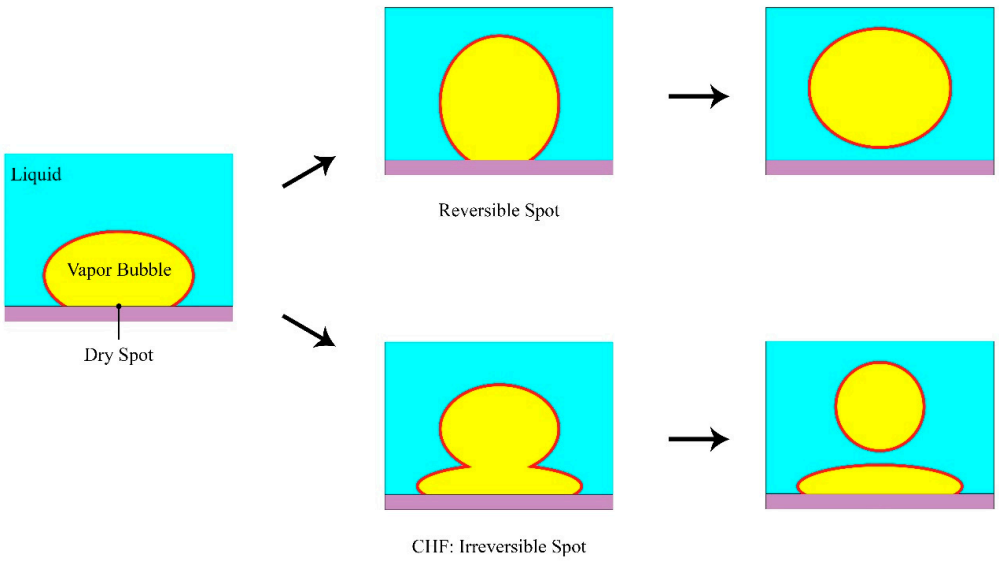

Figure 15. Schematic of a CHF model according to the theory of irreversible dry spot. Adapted from Liang and Mudawar. Reproduced from [252], Elsevier: 2018.

Accordingly, Yagov [239] developed diverse CHF correlations for various ranges of diminished pressure. For small diminished pressures $\left(\frac{P}{P_c} < 0.001\right)$, one can express:

$$q''_{CHF,l} = 0.5\frac{h_{fg}^{81/55}\sigma^{9/11}\,\rho_g^{13/110}\,k_f^{7/110}\,g^{21/55}\,f\left(Pr_f\right)}{v_f^{1/2}\,C_{P,f}^{3/10}\,R_i^{79/110}\,T_{sat}^{21/22}} \tag{11}$$

where the subscripts of g, f and sat are respective expressions for gas, fluid and saturation, while h, σ, ρ, k, g, v, C_P and T stand for latent heat, liquid vapor interface tension, density, thermal conductivity, gravitational acceleration, kinematic viscosity, specific heat capacity and temperature, respectively. Moreover, R_i shows the individual gas constant, and the Prandtl number function $f\left(Pr_f\right)$ can be determined by:

$$f\left(Pr_f\right) = \left(\frac{{Pr_f}^{9/8}}{1 + 2{Pr_f}^{1/4} + 0.6{Pr_f}^{19/24}}\right)^{\frac{4}{11}} \tag{12}$$

where the subscript of f stands for fluid and Pr denotes Prandtl number. For high reduced pressures $\left(\frac{P}{P_c} > 0.03\right)$, the following equation can be stated:

$$q''_{CHF,h} = 0.06\,h_{fg}\,\rho_g^{3/5}\,\sigma^{2/5}\left[\frac{g\left(\rho_f - \rho_g\right)}{\mu_f}\right]^{\frac{1}{5}} \tag{13}$$

where the subscripts of f and g are respective expressions for fluid and gas, while h, ρ, σ, g and μ stand for latent heat, density, liquid vapor interface tension, gravitational acceleration and dynamic viscosity, respectively. The following weighting function was suggested by Yagov [239] to obtain the CHF for intermediately diminished pressures, $\left(0.001 \le \frac{P}{P_c} \le 0.03\right)$:

$$q''_{CHF} = \left(q''^3_{CHF,hp} + q''^3_{CHF,lp}\right)^{\frac{1}{3}} \tag{14}$$

where the subscripts of hp and lp denote high pressure and low pressure, respectively. Notably, in contrary to the hydrodynamic instability model, the dry spot model is dependent on liquid viscosity. The impact of viscosity will be pronounced at lower pressures (Equations (11) and (12)) while getting much weaker at high pressures (Equation (13)). Yagov [239] concluded that Equation (13) predicts CHF values closer to the results of hydrodynamic instability models since the majority of experiments were conducted at moderate to high reduced pressures in which the influence of viscosity was rather weak. Kam et al. [253] developed the observation-based model by dividing the dry patch into two kinds of reversible (quenchable) or irreversible (unquenchable).

4.4.2. Theofanous and Dinh Formulation

With the help of a high-speed, high resolution infrared imaging, Theofanous et al. [240,254] reported a temperature pattern on the surface during nucleate boiling. Lower temperatures were observed at cold spots (known as active nucleation sites), which might be due to effective heat removal by the bubble growth. By elevation of the heat flux, the cold spot pattern got more regular, despite an augmentation in the pool's two-phase motion chaos. Moreover, enhancement of the heat flux will result in the development of the hot spots inside the originally cold spots; at this time, CHF will be initiated by irreversible growth of hot spots, as illustrated in Figure 16. Moreover, Jung et al. [255] expressed that CHF occurrence is upon the faster growth of dry spot size compared to the heat transfer increment through the wetted area; thus, higher CHF is achievable by either the enhancement of the wetted fraction of the surface or improvement of heat transfer within the wetted parts.

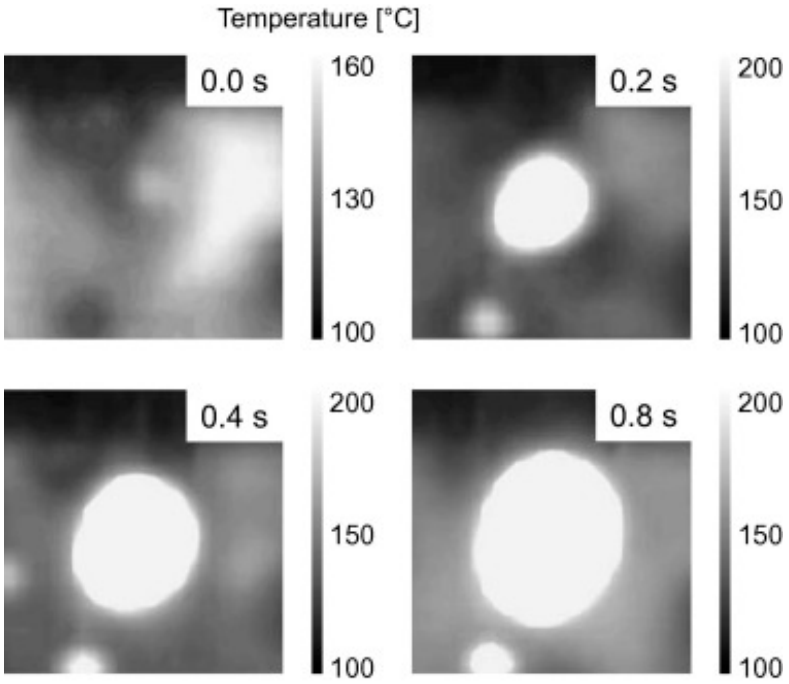

Figure 16. Demonstration of dry-spot development at CHF for water. Reproduced from [253], Elsevier: 2002.

Presuming that CHF is governed by the liquid microlayer dynamics and instability, a follow-up investigation by Theofanous and Dinh [256] resulted in a CHF relation similar to that of Kutateladze–Zuber:

$$q''_{CHF} = k^{-\frac{1}{2}}\,\rho_g h_{fg}\left[\frac{\sigma g\left(\rho_f - \rho_g\right)}{\rho_g^2}\right]^{\frac{1}{4}} \tag{15}$$

In the above relation, k denotes a function of surface conditions that descend by an increase in the surface wettability. No approach was, however, proposed to calculate this parameter. An analytical equation was then developed for *k* by Kim et al. [102] based on Lord Rayleigh's formula for a volume of static liquid meniscus [257]:

$$k = \left(1 - \frac{\sin\theta}{2} - \frac{\frac{\pi}{2} - \theta}{2\cos\theta}\right)^{-\frac{1}{2}} \tag{16}$$

The above relation can be applied for hydrophilic surfaces, whose contact angles are less than 90°.

4.4.3. Other Observations

On the basis of the total reflection technique, Chu et al. [258] lately proved that, in contrast to the general belief in the presence of a thin, stable liquid film beneath large coalescent hovering bubbles, these bubbles reside on an almost dry surface even prior to CHF onset. The hydraulic and thermal criteria were developed by Choi et al. [259] for the irreversible dry spot initiation. Based on the hydraulic criterion, the irreversible condition occurs in cases where the number of dry spots grows to a critical level, at which point the spots are in contact with each other. According to the thermal criterion, the irreversible condition initiates when the temperature of dry spot environment reaches the Leidenfrost temperature preventing the surface rewetting even after the bubble departure. The CHF is achievable upon the fulfillment of both criteria. Kim et al. [260] observed that the irreversible dry spots will be formed in water at 134 °C, which is far lower than the Leidenfrost and maximum liquid-contact temperatures. Kim et al. [260] and Chu et al. [261] agreed that an irreversible dry spot will be formed

as the consequence of vigorous bubble nucleation close to the triple phase contact line, which will prevent from the dry spot wetting.

Advances to stronger flow visualization and measurement methods will drastically improve readers' insight into interfacial mechanisms near the dry spot. This will further enhance the dry-spot-based CHF model's prediction capabilities.

4.5. Interfacial Lift-Off Model

4.5.1. Vertical and Near-Vertical Orientations

Galloway and Mudawar [262] conducted a high-speed video motion investigation and hypothesized that CHF within flow boiling occurs upon sufficient growth of vapor momentum in a way that it can lift the bulk liquid away from the surface. They applied this mechanism to develop a phenomenological interfacial lift-off model [263]. Subsequently, Mudawar et al. [264,265] reported the similarity of the CHF interfacial behavior in pool boiling along the vertical surface to the flow boiling CHF. Based on pool boiling illustrations, a series of incidents will cause the CHF. In cases where heat flux is slightly less than CHF, intensive vaporization may lead to the formation of a vapor layer propagating along the surface. Considerable waves may be formed in this layer as the result of Helmholtz instability which allow liquid contact with the surface only in the 'wetting fronts' corresponding to the wave troughs. The mentioned wetting fronts sweep along the surface and provide the last opportunity for the surface cool down. CHF can be regarded as a consequence of wetting front loss in cases where the severe surface-perpendicular vapor momentum rises beyond the opposing interfacial curvature-induced pressure force.

$$\rho_g \left[\frac{q_l''}{\rho_g h_{fg} \left(1 + \frac{C_{P,f} \Delta T_{sub}}{h_{fg}} \right)} \right]^2 = \overline{\rho_f - \rho_g} \tag{17}$$

where q_l'' denotes the localized heat flux within the wetting front. Additionally, subscripts of g, f and sub are respective expressions for gas, fluid and subcooled, while ρ, h, C_P and T stand for density, latent heat, specific heat capacity and temperature, respectively. The average interfacial curvature-induced pressure difference can be determined by:

$$\overline{\rho_f - \rho_g} = 2\sqrt{2}\pi \frac{\sigma \delta}{\gamma_c^2} \tag{18}$$

where δ represents the mean vapor layer thickness, whereas σ stands for liquid vapor interface tension; γ_c is the critical wavelength corresponding to the initiation of the Helmholtz instability. By the substitution of Equation (18) in Equation (17) and considering the wetting front span as $\frac{1}{4}$ of the critical wavelength (i.e., $q_{CHF}'' = q_l''/4$), one can present:

$$q_{CHF}'' = \frac{1}{4} \rho_g h_{fg} \left(1 + \frac{C_{P,f} \Delta T_{sub}}{h_{fg}} \right) \left[2\sqrt{2}\pi \frac{\sigma \delta}{\rho_g \gamma_c^2} \right]^{\frac{1}{2}} \tag{19}$$

Different flow models were used to derive the analytical equations of δ and γ_c:

$$\delta = \frac{q_{CHF}''}{\rho_g h_{fg} \left(1 + \frac{C_{P,f} \Delta T_{sub}}{h_{fg}} \right)} \left[g \left(\frac{\rho_f - \rho_g}{\rho_g} \right) \frac{q_{CHF}''}{0.5\, f_i\, \rho_g h_{fg} \left(1 + \frac{C_{P,f} \Delta T_{sub}}{h_{fg}} \right)} \right]^{\frac{1}{3}} \gamma_c^{2/3} \tag{20}$$

where

$$\gamma_c = \left[2\pi\sigma\left(\frac{\rho_f + \rho_g}{\rho_f\,\rho_g}\right)\right]^{\frac{3}{5}}\left[g\left(\frac{\rho_f - \rho_g}{\rho_g}\right)\frac{q''_{CHF}}{0.5\,f_i\,\rho_g h_{fg}\left(1 + \frac{C_{P,f}\Delta T_{sub}}{h_{fg}}\right)}\right]^{-\frac{2}{5}} \quad (21)$$

In the above equation, f_i denotes the interfacial friction factor (considered as 0.5). By the substitution of Equations (20) and (21) in Equation (19), the following equation will be obtained:

$$q''_{CHF} = 2^{-113/24}\,3^{5/6}\left(\frac{\pi}{f_i}\right)^{1/4}\left(\frac{\rho_f}{\rho_f + \rho_g}\right)\rho_g h_{fg}\left(1 + \frac{C_{P,f}\Delta T_{sub}}{h_{fg}}\right)\left[\frac{\sigma g\left(\rho_f - \rho_g\right)}{\rho_g^2}\right]^{\frac{1}{4}} \quad (22)$$

Under saturated condition and for noncritical pressure values, the mentioned equation could be further simplified as:

$$q''_{CHF} = 0.151\,\rho_g h_{fg}\left[\frac{\sigma g\left(\rho_f - \rho_g\right)}{\rho_g^2}\right]^{\frac{1}{4}} \quad (23)$$

Equation (23) is similar to the Kutateladze–Zuber equation. Notably, the gravity term in Equation (23), however, originates from the buoyancy-driven vapor flow rather than the Taylor instability in Zuber's model. Subsequent studies by Howard and Mudawar [265] showed that the CHF interfacial lift-off trigger process is not restricted to the vertical orientation, as it encompasses all the near-vertical orientations varying in θ = 60–165° (see Figures 17b and 18). The mentioned model can effectively predict the near-vertical-downward-facing transition angle of 165°, as illustrated in Figure 19. By the application of various reported data, they also indicated that, at $0 < \theta < 90°$, the impact of orientation on CHF is very weak, implying that Equation (23) is equally valid for $h = 0°$ and 90°. Recent studies by Kim et al. [266] and Zhong et al. [267] also confirmed the interfacial lift-off model in pool boiling CHF with various orientations.

The interfacial lift-off model is highly versatile and precise in the prediction of flow boiling CHF at diverse conditions, including microgravity [268,269]. In particular, it confirms the gravity dependence of CHF. Overall, in comparison with pool boiling, it is more successful in the prediction of decreased gravity CHF for flow boiling [270].

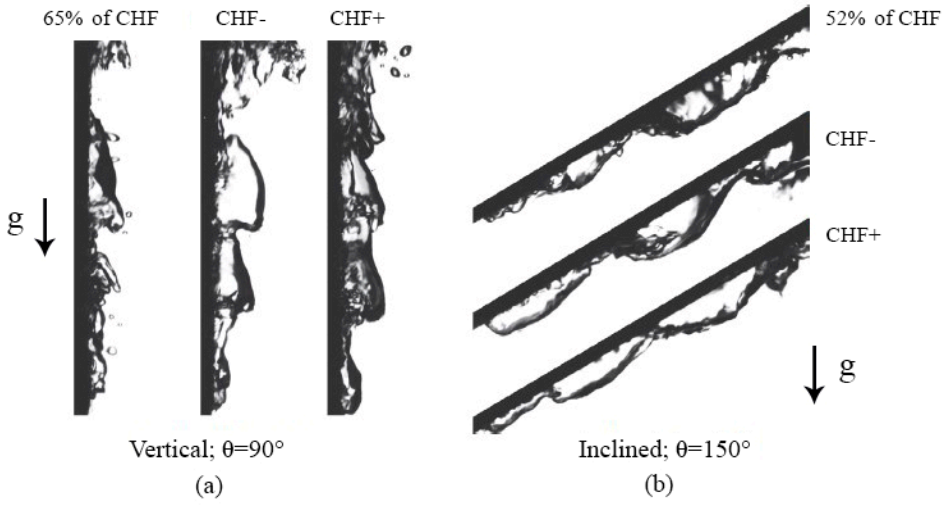

Figure 17. Pool boiling photographs for ameliorating heat flux at diverse surface orientations of (**a**) θ = 90° and (**b**) θ = 150°. Adapted from Howard and Mudawar. Reproduced from [265], Elsevier: 1999.

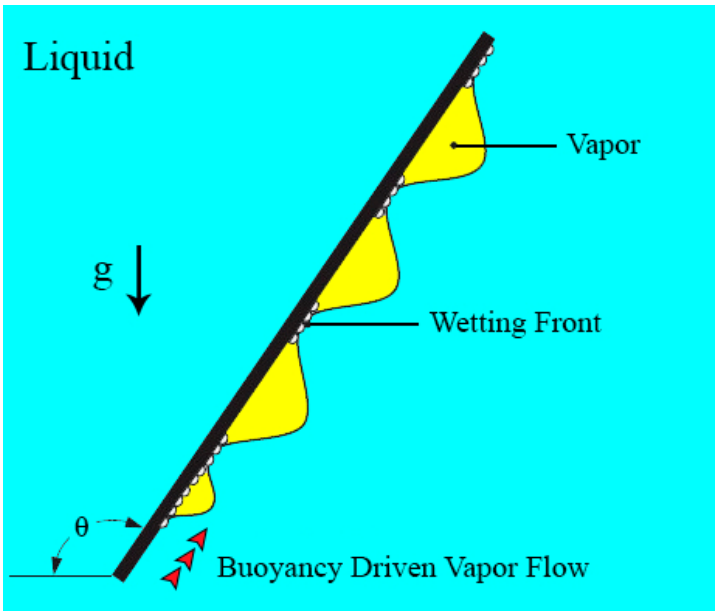

Figure 18. Illustration of interfacial lift-off CHF model on a near perpendicular surface in pool boiling. Adapted from Howard and Mudawar. Reproduced from [265], Elsevier: 1999.

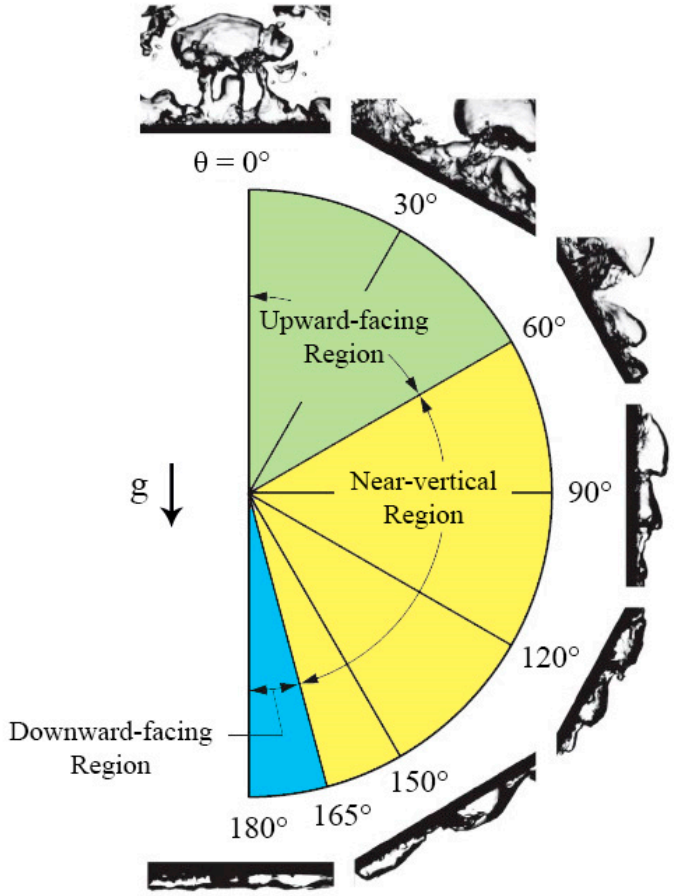

Figure 19. Pool boiling images and regions of various CHF mechanisms at diverse surface orientations. Adapted from Liang and Mudawar. Reproduced from [252], Elsevier: 2018.

4.5.2. Horizontal, Upward-Facing Orientation

The interfacial lift-off process in pool boiling CHF was also addressed along with the upward-facing orientation by Guan et al. [271]. The lift-off process for pentane is illustrated in Figure 20 through a series of images. At $t = 0$ s, a small vapor patch can be seen at the right edge of the surface which propagated from right to left until $t = 2.8$ s when the whole surface was covered by vapor. Accordingly, they proposed a CHF model for pool boiling on the basis of a liquid macrolayer lift-off process, which relies on the Galloway's and Mudawar's interfacial lift-off model [263]. The major difference is that the Guan et al. [271] model (Figure 21) does not require a separate flow model for the determination of the vapor layer parameters. It rather employs the momentum conservation and Laplace condition on the vapor–liquid interface to obtain an equation for CHF-corresponding upward vapor velocity.

$$u_g = \sqrt{\frac{2\sigma}{r\rho_g}} \tag{24}$$

In the above equation, r represents the local interface curvature radius. Maximum vapor velocity can be achieved at minimal local radius:

$$r = \sqrt{\frac{\lambda_d^2}{2\pi^2\delta^*}} \tag{25}$$

where δ^* shows the liquid macrolayer thickness predictable by the theoretical formulation proposed by Rajvanshi et al. [272]. Using this approach, the following equation can be obtained for pool boiling CHF:

$$q''_{CHF} = \rho_g u_g h_{fg} = 0.2445\left(1 + \frac{\rho_g}{\rho_f}\right)^{\frac{1}{4}}\left(\frac{\rho_g}{\rho_f}\right)^{\frac{1}{10}}\rho_g h_{fg}\left[\frac{\sigma g\left(\rho_f - \rho_g\right)}{\rho_g^2}\right]^{\frac{1}{4}} \tag{26}$$

The above equation is relatively similar to the Kutateladze–Zuber equation.

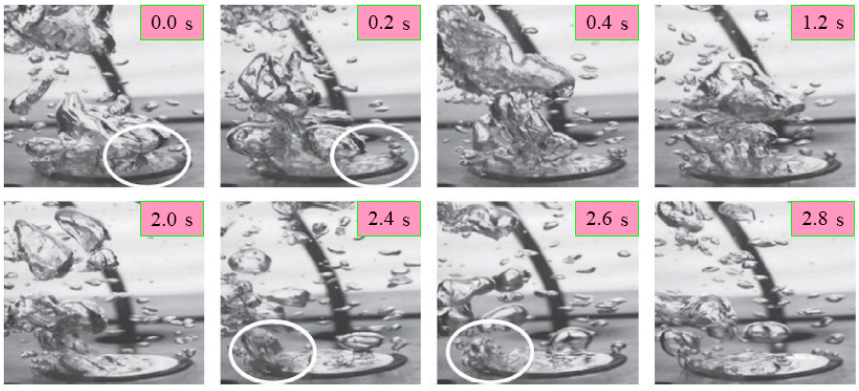

Figure 20. Demonstration of interfacial lift-off in pool boiling process for pentane at $\Delta T_{sat} = 20$ °C and $P_g = 150$ kPa. Reproduced from [271], Elsevier: 2011.

Altogether, the interfacial lift-off mechanism for pool boiling CHF relies on microscopic observation with phenomenological appeals that may not be found in the experimental CHF correlations. Moreover, owing to its dependence on hydrodynamic instability theory, it will result in a dimensionless formulation similar to the Kutateladze–Zuber equation.

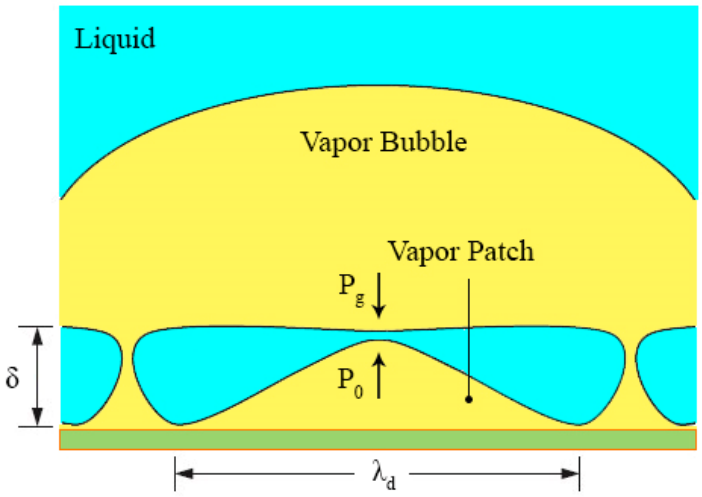

Figure 21. Macrolayer lift-off illustration during CHF from a horizontal upward-facing surface [271]. Reproduced from [271], Elsevier: 2011.

5. Challenges and Suggestions

Based on the review of available studies, enhanced CHF not only increases heat transfer efficiency but also augments the safety of heat management. A wide diversity of pool boiling experiments have been carried out at various concentrations, preparation methods and nanofluids stabilities to significantly enhance the CHF. Furthermore, different surface properties, including porosity, capillarity, wettability and roughness, can increase CHF through a complicated mechanism. CHF can be also elevated through modifying flow channel by either altering its size or incorporating surface modifiers. The application of hybrid or hierarchical structures can substantially improve the CHF for some particular purposes, among which the hydrophilic membrane with micro-channels and a combination of high porosity with the super-hydrophilic nature of the surface can be mentioned. Moreover, CHF is under the substantial influence of surface wettability and capillary wicking. The synergetic impact of the mentioned parameters should be extensively examined for diverse nanoparticle sizes and concentrations to elucidate the mechanism of CHF amelioration. Despite a wide diversity in boiling heat transfer theories to explain the variations in nanofluids' properties and surface wettability, no comprehensive theory has been introduced to mechanistically justify the CHF amelioration for a wide spectrum of nanoparticle size and contents. A lack of such an inclusive framework has limited the nanofluids commercialization in various fields including nuclear reactor, fossil fuel boiler, spray cooling and high-power electronics. Resolving the key issues can pave the way for experiments on thermal engineering systems. Researchers have recognized the nanoparticle deposition-induced enhancement in surface wettability and capillarity as the main cause of CHF augmentation. Table 2 summarizes the impacts on nanofluids' CHF.

Table 2. Summary of the parameter variation impacts on CHF.

Parameter Variations	CHF	Reason
Increase in the surface roughness	Increase	The CHF causes a higher surface superheat. The efficient contact area increases.
Increase in the surface wettability	Increase	The liquid traps in the porous structure and the vapour layer formation is prevented. The number of active nucleation sites decreases because of the low contact angle and the vapour layer formation is prevented.
Increase in the capillarity	Increase	The dry regions under the vapour bubbles are wetted by fresh liquid.

So far, several questions have remained unanswered. Thus, highly creative and practical investigations are required to establish the advanced approaches for CHF amelioration. The following recommendations can be considered for further understanding the fundamental mechanisms of CHF amelioration:

(1) Despite the relative maturity of nanofluid-related studies, issues such as long-period stability, probable erosion and required maintenance measures as well as cleaning procedures have remained obstacles to nanofluid commercialization. In this context, studies to extend the available predictive correlations or numerical simulation tools for CHF prediction are highly encouraged. Furthermore, the next generation of nanofluids, including shell-core nanofluids, microfluidics and hybrids of more than two nanofluids, are interesting topics owing to their phase-change characteristics and optimized thermo-physical properties, which may result in higher heat transfer efficiency and outstanding stability.

(2) Regarding the depositing tendency of nanofluids during boiling, texture fabrications and coating particles on the surface have been intensively explored to improve CHF. The probable micro/nanostructure detachment or failure during the boiling process needs to be further addressed experimentally. Moreover, in the case of applying nanotubes or nanowires as the coating substance, the choking issue must be avoided by the systematic optimization of their diameter and length. Besides, the complexity of the surface properties' relationships should be addressed to further clarify the fundamental mechanisms of CHF amelioration.

(3) In spite of huge improvements to surface modifications for flow boiling, a considerable gap still remains between the studies and engineering applications, particularly considering the size of system. Large engineering scales with different shapes were explored by micro-channels, making the coating process an obstacle in practical engineering scales.

(4) The literature review showed that the integration of hybrid and hierarchical structures can significantly enhance the CHF. It is, however, accompanied by difficulties for separately investigating the impact of surface features on CHF amelioration. Putting the safe CHF enhancement as the major objective, the integration of advanced approaches, such as acoustic methods, magnetic fields and other creative techniques through novel preparation methods and materials are highly recommended.

(5) Nanofluid stability has remained one of the major challenges. Instead of experimental studies with varying mass fractions, various approaches have been tested (i.e., pH control, surfactants and surface functionalization) to prevent from nanoparticles' agglomeration and sedimentation, which are, albeit, at a research level. In this regard, the industrial application of nanofluids will be realized only when their long-term physical and chemical stabilities are guaranteed at the mass production level.

(6) Nanoparticle size is another important factor in the heat transfer field. The use of smaller nanoparticles is recommended. Thus, cost-effective synthesis methods should be established to prepare relatively small nanoparticles.

(7) The relative size effect of nanoparticles in the liquid phase requires further examination to prevent from particle clustering.

(8) To the best of our knowledge, a limited number of studies have attributed the CHF amelioration to alternations in nanofluids' thermal transport properties. Therefore, a database including the thermal transport characteristics along with the detailed specification of nanoparticle sizes and dispersion stability with/without surfactant is recommended, in which the promising nanofluids are prioritized.

(9) Regarding the key role of the deposited layer on the heating surface in CHF amelioration, the thickness should be optimized to induce the maximum latency in the CHF occurrence. Moreover, the stability of the deposited layer should be experimentally checked in several replications.

(10) The synergetic impact of surface wettability and capillary wicking should be addressed to mechanistically elucidate the CHF enhancement for various particle sizes and concentrations.
(11) Application of nano-coats on the heating surface by the physical/chemical vapor deposition method is a promising approach compared to nanofluids. This technique, however, demands extensive investigations regarding its stability and optimal thickness to examine the delay in the CHF occurrence.
(12) The bubble dynamics should be empirically and numerically examined to determine the exact share of deposited layer and nanoparticle in the CHF amelioration.
(13) Regarding the significance of pressure, the irreversible growth of dry patches should be explored at various pressure levels to elucidate the CHF enhancement in nanoparticles deposited layer.

6. Concluding Remarks

The present study is an overview on the CHF amelioration of pool boiling surfaces through the use of metal oxide nanoparticles deposition. The impact of metal oxide nanoparticles and their thermo-physical properties, concentration, shape and size were addressed and the inconsistencies or conflicts in the available literature were highlighted. In addition, nanoparticle deposition techniques were reviewed to find an efficient substitution for deposition rather than nanofluid boiling. Moreover, possible mechanisms and models were discussed to explore the enhancement findings. This review study had the following observations:

(1) Besides the innovative dimensional analysis-based Kutateladze's CHF formulation, five different CHF mechanisms have been widely employed: bubble interference, hydrodynamic instability, macrolayer dry-out, hot/dry spot, and interfacial lift-off, among which the Zuber's hydrodynamic instability theory has gained the highest popularity owing to its mechanistic formulation and theoretical attractiveness. Lately, the theoretical-based interfacial lift-off mechanism has been widely confirmed by experimental results that can deal with various surface orientations.
(2) The impacts of thermo-physical properties, concentration, shape and size on CHF have been extensively addressed in heat transfer field. Accordingly, CHF rises with wall thickness enhancement but reaches an asymptotic value beyond a thickness threshold. Thus, the data corresponding to wall thicknesses beyond this threshold are highly essential. Altogether, a limited amount of data covers the entire relevant parameters of the fluids with various thermal features. A severe shortage is also felt regarding the horizontal, downward-facing surface orientations reflecting the need for more advanced strategies to plan the future studies including the micro-photographic analysis of near-wall interfacial phenomena to confirm or reject the introduced CHF mechanism.
(3) Considering the complexity of the CHF phenomenon and its dependence on a diverse range of factors, the available data should be combined in a comprehensive database to assess diverse models and correlations. Such database will be expanded by the inclusion of new data to fill the vacancies regarding the relevant parameters.
(4) Nanofluids can undoubtedly improve the CHF, which can be attributed to the enhanced surface wettability upon nanoparticles deposition. The data regarding the impact of nanofluids on nucleate boiling HTC are, however, contradictory, which may be due to involvement of numerous complex factors, such as the type of liquid, initial surface roughness, and heat flux in addition to nanoparticle type, size, concentration, preparation and functionalization procedure, which can substantially affect the thermo-physical characteristics of the nanofluid and surface characteristics (i.e., surface finish, active nucleation site density, wettability and changes in the triple line). Such complexities can definitely restrict the theoretical attempts to model the nanofluid boiling.
(5) Bath quenching the metal portion of a nanofluid is related to the cooling rates similar to, or even weaker than, those of the base liquid. The cooling rate can be accelerated by successive quenching as it will thicken the nanoparticle layer on the surface. At elevated surface temperatures,

this layer will further destabilize the vapor film, leading to the premature disruption of the film boiling pattern.

(6) The nanofluid-induced nucleate boiling enhancement can be attributed to nanoparticle deposition on the surface, resulting in capillary wicking in the porous layer and enhancement in surface wettability and bubble dynamics. These impacts are competing with each other depending on the size of nanoparticles relative to the surface roughness.

(7) Although the nanofluids have shown high potentials in improving the boiling performance, some practical issues should be closely considered prior to the utilization of nanofluids in practical cooling purposes, among which the clustering, sedimentation and precipitation of nanoparticles, the clogging of intricate features, the heating surface erosion of the temporal variation of cooling performance, and the cost of quality can be mentioned.

(8) Despite the improving impacts of nanofluids on the thermal conductivity of the boiling fluid, the majority of their usefulness is rooted in their surface modification. Other approaches of surface modifications (such as micro/nano studs, nanotube/nanowire arrays, microporous structure, and nanoparticle pre-deposition) are capable of offering comparable or even better heat transfer enhancements with no practical problems relevant to use of nanofluid boiling.

Author Contributions: H.M., N.M.; Conceptualization, Writing—Original Draft Preparation, Writing—Review & Editing, A.M.G.; Writing—Review & Editing, H.S.; Supervision & Project Administration, G.Q.Z.; Project Administration. All authors have read and agreed to the published version of the manuscript.

Funding: This research received no external funding.

Conflicts of Interest: The authors declare no conflict of interest.

Nomenclature

b	Channel half-spacing (m)
C_P	Specific heat capacity $\left(\frac{\mathrm{J}}{\mathrm{kg\ K}}\right)$
f_i	Interfacial friction factor
g	Gravitational acceleration $\left(\frac{\mathrm{m}}{\mathrm{s}^2}\right)$
h	Heat transfer coefficient $\left(\frac{\mathrm{W}}{\mathrm{m}^2\ \mathrm{K}}\right)$
h_{fg}	Latent heat of evaporation $\left(\frac{\mathrm{kJ}}{\mathrm{kg}}\right)$
j	Superficial velocity $\left(\frac{\mathrm{m}}{\mathrm{s}}\right)$
l	Channel height (m)
L	Rise of liquid (m)
n	Active nucleation site density $\left(\frac{1}{\mathrm{m}^2}\right)$
P	Pressure (Pa)
q	Heat transfer (kJ)
r	Local radius of curvature of the interface (m)
R	Micro/nano structured surface (m)
R_i	Individual gas constant $\left(\frac{\mathrm{J}}{\mathrm{mol\ K}}\right)$
T	Temperature (K)
u	Velocity $\left(\frac{\mathrm{m}}{\mathrm{s}}\right)$

Greek symbols

γ	Wavelength (m)
δ	Mean vapor layer thickness (m)
δ^*	Liquid macrolayer thickness (m)
θ	Contact angle (deg)
λ	Thermal conductivity $\left(\frac{\mathrm{W}}{\mathrm{m\cdot K}}\right)$
μ	Dynamic viscosity (Pa s)
ν	Kinematic viscosity $\left(\frac{\mathrm{m}^2}{\mathrm{s}}\right)$

ρ	Density $\left(\frac{\text{kg}}{\text{m}^3}\right)$
σ	Liquid vapor interface tension $\left(\frac{\text{N}}{\text{m}}\right)$
τ	Time (s)
ϕ	Concentration

Subscript

bf	Base fluid
cri	Critical
d	Departure
f	Fluid
g	Gas
hp	High pressure
l	Liquid
lp	Low pressure
nf	Nano-fluid
sat	Saturation
sub	Subcooled
v	Vapor
w	Wall
∞	Ambient fluid

Abbreviation

AFM	Atomic force microscopy
CHF	Critical heat flux $\left(\frac{\text{W}}{\text{m}^2}\right)$
CNC	Computer numerical control
CNT	Carbon nano tube
DNB	Departure from nucleate boiling
EG	Ethylene glycol
HTC	Heat transfer coefficient $\left(\frac{\text{W}}{\text{m}^2\,\text{K}}\right)$
MWNF	Magnetite-water nanofluids
ONB	Onset of nucleate boiling
Pr	Prandtl number
PVA	Polyvinyl alcohol
RGO	Reduced graphene oxide
SLBS	Sodium lauryl benzene sulphonate
SLS	Sodium lauryl sulfate
TEM	Transmission electron microscopy
TIM	Thermal interface material
TSP	Tri-sodium phosphate

References

1. Moghadasi, H.; Saffari, H.; Malekian, N. Experimental and semi-analytical investigation of heat transfer in nucleate pool boiling by considering surface structuring methods. *Exp. Heat Transf.* **2020**, 1–21. [CrossRef]
2. Kumar, A.; Hung, K.-S.; Wang, C.-C. Nucleate pool boiling heat transf. from high-flux tube with dielectric Fluid HFE-7200. *Energies* **2020**, *13*, 2313. [CrossRef]
3. Swain, S.; Swain, A.; Kar, S.P. Influence of different surface coatings on pool boiling heat transfer enhancement: A brief review. *Mater. Today Proc.* **2020**, *26*, 1903–1907. [CrossRef]
4. Mehdikhani, A.; Moghadasi, H.; Saffari, H. An exp. investigation of pool boiling augmentation using four-step electrodeposited micro/nanostructured porous surface in distilled water. *Int. J. Mech. Sci.* **2020**, *187*, 105924. [CrossRef]
5. Orman, Ł.J.; Radek, N.; Pietraszek, J.; Szczepaniak, M. Analysis of enhanced pool boiling heat transfer on laser—Textured surfaces. *Energies* **2020**, *13*, 2700. [CrossRef]
6. Liang, G.; Chen, Y.; Yang, H.; Li, D.; Shen, S. Nucleate boiling heat transfer and critical heat flux (CHF) from micro-pit surfaces. *Int. J. Heat Mass Transf.* **2020**, *152*, 119510. [CrossRef]

7. Hernandez, R.; Folsom, C.P.; Woolstenhulme, N.E.; Jensen, C.B.; Bess, J.D.; Gorton, J.P.; Brown, N.R. Review of pool boiling critical heat flux (CHF) and heater rod design for CHF experiments in TREAT. *Prog. Nucl. Energy* **2020**, *123*, 103303. [CrossRef]
8. Todreas, N.E.; Kazimi, M.S. *Nuclear Systems Volume I: Thermal Hydraulic Fundamentals*; CRC Press: Boca Raton, FL, USA, 2011.
9. Tetreault-Friend, M.; Azizian, R.; Bucci, M.; McKrell, T.; Buongiorno, J.; Rubner, M.; Cohen, R. Critical heat flux maxima resulting from the controlled morphology of nanoporous hydrophilic surface layers. *Appl. Phys. Lett.* **2016**, *108*, 243102. [CrossRef]
10. Choi, K.-Y.; Moon, S.-K.; Chun, S.-Y.; Park, J.-K.; Hwang, D.-H.; Baek, W.-P.; Park, S.-K.; Lee, C.-Y. Critical heat flux tests for an application of the three-pin fuel test loop in HANARO. *Heat Transf. Eng.* **2008**, *29*, 685–694. [CrossRef]
11. Guo, Z.-Y.; Wu, X.-B. Thermal drag and critical heat flux for natural convection of air in vertical parallel plates. *Heat Transf. Eng.* **1993**, *115*, 124–129. [CrossRef]
12. Wu, J.; Zhao, J. A review of nanofluid heat transfer and critical heat flux enhancement—research gap to engineering application. *Prog. Nucl. Energy* **2013**, *66*, 13–24. [CrossRef]
13. Yu, W.; France, D.; Wambsganss, M.; Hull, J. Two-phase pressure drop, boiling heat transfer, and critical heat flux to water in a small-diameter horizontal tube. *Int. J. Multiph. Flow* **2002**, *28*, 927–941. [CrossRef]
14. Dhillon, N.S.; Buongiorno, J.; Varanasi, K.K. Critical heat flux maxima during boiling crisis on textured surfaces. *Nat. Commun.* **2015**, *6*, 8247. [CrossRef] [PubMed]
15. Xie, S.; Beni, M.S.; Cai, J.; Zhao, J. Review of critical-heat-flux enhancement methods. *Int. Commun. Heat Mass Transf.* **2018**, *122*, 275–289. [CrossRef]
16. June Zhang, B.; Kim, K.J. Effect of liquid uptake on critical heat flux utilizing a three dimensional, interconnected alumina nano porous surfaces. *Appl. Phys. Lett.* **2012**, *101*, 054104. [CrossRef]
17. Sarangi, S.; Weibel, J.A.; Garimella, S.V. Effect of particle size on surface-coating enhancement of pool boiling heat transfer. *Int. J. Heat Mass Transf.* **2015**, *81*, 103–113. [CrossRef]
18. Ji, X.; Xu, J.; Zhao, Z.; Yang, W. Pool boiling heat transfer on uniform and non-uniform porous coating surfaces. *Exp. Therm. Fluid Sci.* **2013**, *48*, 198–212. [CrossRef]
19. Ahmadi, A.A.; Khodabandeh, E.; Moghadasi, H.; Malekian, N.; Akbari, O.A.; Bahiraei, M. Numerical study of flow and heat transfer of water-Al 2 O 3 nanofluid inside a channel with an inner cylinder using Eulerian–Lagrangian approach. *Therm. Anal. Calorim.* **2018**, *132*, 651–665. [CrossRef]
20. Malekian, S.; Fathi, E.; Malekian, N.; Moghadasi, H.; Moghimi, M. Analytical and numerical investigations of unsteady graphene oxide nanofluid flow between two parallel plates. *Int. J. Thermophys.* **2018**, *39*, 100. [CrossRef]
21. Farhangmehr, V.; Moghadasi, H.; Asiaei, S. A nanofluid MHD flow with heat and mass transfers over a sheet by nonlinear boundary conditions: Heat and mass transfers enhancement. *J. Cent. South. Univ.* **2019**, *26*, 1205–1217. [CrossRef]
22. Aminian, E.; Moghadasi, H.; Saffari, H. Magnetic field effects on forced convection flow of a hybrid nanofluid in a cylinder filled with porous media: A numerical study. *J. Therm. Anal. Calorim.* **2020**, 1–13. [CrossRef]
23. Moghadasi, H.; Aminian, E.; Saffari, H.; Mahjoorghani, M.; Emamifar, A. Numerical analysis on laminar forced convection improvement of hybrid nanofluid within a U-Bend pipe in porous media. *Int. J. Mech. Sci.* **2020**, *179*, 105659. [CrossRef]
24. Takabi, B.; Gheitaghy, A.M.; Tazraei, P. Hybrid water-based suspension of Al2O3 and Cu nanoparticles on laminar convection effectiveness. *J. Thermophys. Heat. Trans.* **2016**, *30*, 523–532. [CrossRef]
25. Raveshi, M.R.; Keshavarz, A.; Mojarrad, M.S.; Amiri, S. Experimental investigation of pool boiling heat transfer enhancement of alumina–water–ethylene glycol nanofluids. *Exp. Therm. Fluid Sci.* **2013**, *44*, 805–814. [CrossRef]
26. Yagnem, A.R.; S, V. Heat transfer enhancement studies in pool boiling using hybrid nanofluids. *Thermochim. Acta* **2019**, *672*, 93–100. [CrossRef]
27. Yang, X.; Liu, Z.-H. A kind of nanofluid consisting of surface-functionalized nanoparticles. *Nanosc. Res. Lett.* **2010**, *5*, 1324. [CrossRef]
28. Yang, X.-F.; Liu, Z.-H. Pool boiling heat transfer of functionalized nanofluid under sub-atmospheric pressures. *Int. J. Therm. Sci.* **2011**, *50*, 2402–2412. [CrossRef]

29. Kiyomura, I.S.; Manetti, L.L.; Da Cunha, A.; Ribatski, G.; Cardoso, E.M. An analysis of the effects of nanoparticles deposition on characteristics of the heating surface and ON pool boiling of water. *Int. J. Heat Mass Transf.* **2017**, *106*, 666–674. [CrossRef]
30. Cao, Z.; Liu, B.; Preger, C.; Wu, Z.; Zhang, Y.; Wang, X.; Messing, M.E.; Deppert, K.; Wei, J.; Sundén, B. Pool boiling heat transfer of FC-72 on pin-fin silicon surfaces with nanoparticle deposition. *Int. J. Heat Mass Transf.* **2018**, *126*, 1019–1033. [CrossRef]
31. Khan, S.A.; Atieh, M.A.; Koç, M. Micro-nano scale surface coating for nucleate boiling heat transfer: A critical review. *Energies* **2018**, *11*, 3189. [CrossRef]
32. Saffari, H.; Fathalizadeh, H.; Moghadasi, H.; Alipour, S.; Hosseinalipour, S.M. Experimental study of pool boiling enhancement for surface structuring with inclined intersected mesochannels using WEDM method on copper surfaces. *Therm. Anal. Calorim.* **2020**, *139*, 1849–1861. [CrossRef]
33. Yao, Z.; Lu, Y.W.; Kandlikar, S.G. Effects of nanowire height on pool boiling performance of water on silicon chips. *Int. J. Therm. Sci.* **2011**, *50*, 2084–2090. [CrossRef]
34. Shi, B.; Wang, Y.-B.; Chen, K. Pool boiling heat transfer enhancement with copper nanowire arrays. *Appl. Therm. Eng.* **2015**, *75*, 115–121. [CrossRef]
35. Gheitaghy, A.M.; Saffari, H.; Ghasimi, D.; Ghasemi, A. Effect of electrolyte temperature on porous electrodeposited copper for pool boiling enhancement. *Appl. Therm. Eng.* **2017**, *113*, 1097–1106. [CrossRef]
36. Gheitaghy, A.M.; Saffari, H.; Zhang, G.Q. Effect of nanostructured microporous surfaces on pool boiling augmentation. *Heat Trans. Eng.* **2019**, *40*, 762–771. [CrossRef]
37. El-Genk, M.S.; Ali, A.F. Enhancement of saturation boiling of PF-5060 on microporous copper dendrite surfaces. *Heat Transf.* **2010**, *132*, 071501. [CrossRef]
38. Seo, G.H.; Hwang, H.; Yoon, J.; Yeo, T.; Son, H.H.; Jeong, U.; Jeun, G.; Choi, W.; Kim, S.J. Enhanced critical heat flux with single-walled carbon nanotubes bonded on metal surfaces. *Exp. Therm. Fluid Sci.* **2015**, *60*, 138–147. [CrossRef]
39. Dharmendra, M.; Suresh, S.; Sujith Kumar, C.S.; Yang, Q. Pool boiling heat transfer enhancement using vertically aligned carbon nanotube coatings on a copper substrate. *Appl. Therm. Eng.* **2016**, *99*, 61–71. [CrossRef]
40. Xu, P.; Li, Q.; Xuan, Y. Enhanced boiling heat transfer on composite porous surface. *Int. J. Heat Mass Transf.* **2015**, *80*, 107–114. [CrossRef]
41. Liter, S.G.; Kaviany, M. Pool-boiling CHF enhancement by modulated porous-layer coating: Theory and experiment. *Int. J. Heat Mass Transf.* **2001**, *44*, 4287–4311. [CrossRef]
42. Wu, W.; Du, J.-H.; Hu, X.-J.; Wang, B.-X. Pool boiling heat transfer and simplified one-dimensional model for prediction on coated porous surfaces with vapor channels. *Int. J. Heat Mass Transf.* **2002**, *45*, 1117–1125. [CrossRef]
43. Mori, S.; Okuyama, K. Enhancement of the critical heat flux in saturated pool boiling using honeycomb porous media. *Int. J. Multiph. Flow* **2009**, *35*, 946–951. [CrossRef]
44. Kim, S.; Kim, H.D.; Kim, H.; Ahn, H.S.; Jo, H.; Kim, J.; Kim, M.H. Effects of nano-fluid and surfaces with nano structure on the increase of CHF. *Exp. Therm. Fluid Sci.* **2010**, *34*, 487–495. [CrossRef]
45. Yao, Z.; Lu, Y.W.; Kandlikar, S.G. Pool boiling heat transf. enhancement through nanostructures on silicon microchannels. *Nanotechnol. Eng. Med.* **2013**, *3*, 031002. [CrossRef]
46. Moon, H.W.; Yoon, Y.J.; Park, J.H.; Myung, B.-S.; Kim, D.E. Dynamic wetting and boiling characteristics on micro-structured and micro/nano hierarchically structured surfaces. *Exp. Therm. Fluid Sci.* **2016**, *74*, 19–26. [CrossRef]
47. Jaikumar, A.; Kandlikar, S.G. Pool boiling enhancement through bubble induced convective liquid flow in feeder microchannels. *Appl. Phys. Lett.* **2016**, *108*, 041604. [CrossRef]
48. Jaikumar, A.; Kandlikar, S.G. Ultra-high pool boiling performance and effect of channel width with selectively coated open microchannels. *Int. J. Heat Mass Transf.* **2016**, *95*, 795–805. [CrossRef]
49. Rahman, M.M.; Ölçeroğlu, E.; McCarthy, M. Role of wickability on the critical heat flux of structured superhydrophilic surfaces. *Langmuir* **2014**, *30*, 11225–11234. [CrossRef]
50. Kandlikar, S. Controlling bubble motion over heated surface through evaporation momentum force to enhance pool boiling heat transfer. *Appl. Phys. Lett.* **2013**, *102*, 051611. [CrossRef]
51. Boziuk, T.R.; Smith, M.K.; Glezer, A. Enhanced boiling heat transfer on plain and featured surfaces using acoustic actuation. *Int. Commun. Heat Mass Transf.* **2017**, *108*, 181–190. [CrossRef]

52. Miner, M.J.; Phelan, P.E.; Odom, B.A.; Ortiz, C.A. Experimental measurements of critical heat flux in expanding microchannel arrays. *Heat Transf.* **2013**, *135*, 101501. [CrossRef]
53. Gheitaghy, A.M.; Samimi, A.; Saffari, H. Surface structuring with inclined minichannels for pool boiling improvement. *Appl. Therm. Eng.* **2017**, *126*, 892–902. [CrossRef]
54. Gheitaghy, A.M.; Saffari, H.; Mohebbi, M. Investigation pool boiling heat transfer in U-shaped mesochannel with electrodeposited porous coating. *Exp. Therm. Fluid Sci.* **2016**, *76*, 87–97. [CrossRef]
55. Bai, L.; Zhang, L.; Lin, G.; Peterson, G. Pool boiling with high heat flux enabled by a porous artery structure. *Appl. Phys. Lett.* **2016**, *108*, 233901. [CrossRef]
56. Joshi, S.N.; Dede, E.M. Two-phase jet impingement cooling for high heat flux wide band-gap devices using multi-scale porous surfaces. *Appl. Therm. Eng.* **2017**, *110*, 10–17. [CrossRef]
57. Tan, L.; Chen, C.; Dong, X.; Gong, Z.; Wang, M. Experimental study on CHF of R134a flow boiling in a horizontal helically-coiled tube near the critical pressure. *Exp. Therm. Fluid Sci.* **2017**, *82*, 472–481. [CrossRef]
58. Bergles, A.; Nirmalan, V.; Junkhan, G.; Webb, R. *Bibliography on Augmentation of Convective Heat and Mass Transfer-II*; Iowa State University of Science and Technology: Ames, IA, USA, 1983.
59. Webb, R.L.; Bergles, A.; Junkhan, G. *Bibliography of US Patents on Augmentation of Convective Heat and Mass Transfer-II*; Iowa State University of Science and Technology: Ames, IA, USA, 1983.
60. Bhavnani, S.; Narayanan, V.; Qu, W.; Jensen, M.; Kandlikar, S.; Kim, J.; Thome, J. Boiling augmentation with micro/nanostructured surfaces: Current status and research outlook. *Nanosc. Microsc. Thermophys. Eng.* **2014**, *18*, 197–222. [CrossRef]
61. Shojaeian, M.; Koşar, A. Pool boiling and flow boiling on micro-and nanostructured surfaces. *Exp. Therm. Fluid Sci.* **2015**, *63*, 45–73. [CrossRef]
62. McCarthy, M.; Gerasopoulos, K.; Maroo, S.C.; Hart, A.J. Materials, fabrication, and manufacturing of micro/nanostructured surfaces for phase-change heat transfer enhancement. *Nanosc. Microsc. Thermophys. Eng.* **2014**, *18*, 288–310. [CrossRef]
63. Kim, D.E.; Yu, D.I.; Jerng, D.W.; Kim, M.H.; Ahn, H.S. Review of boiling heat transfer enhancement on micro/nanostructured surfaces. *Exp. Therm. Fluid Sci.* **2015**, *66*, 173–196. [CrossRef]
64. Attinger, D.; Frankiewicz, C.; Betz, A.R.; Schutzius, T.M.; Ganguly, R.; Das, A.; Kim, C.-J.; Megaridis, C.M. Surface engineering for phase change heat transfer: A review. *MRS Energy Sustain.* **2014**, *1*. [CrossRef]
65. Honda, H.; Wei, J. Enhanced boiling heat transfer from electronic components by use of surface microstructures. *Exp. Therm. Fluid Sci.* **2004**, *28*, 159–169. [CrossRef]
66. Lu, Y.-W.; Kandlikar, S.G. Nanoscale surface modification techniques for pool boiling enhancement—A critical review and future directions. *Heat Transf. Eng.* **2011**, *32*, 827–842. [CrossRef]
67. Patil, C.M.; Kandlikar, S.G. Review of the manufacturing techniques for porous surfaces used in enhanced pool boiling. *Heat Transf. Eng.* **2014**, *35*, 887–902. [CrossRef]
68. Mori, S.; Utaka, Y. Critical heat flux enhancement by surface modification in a saturated pool boiling: A review. *Int. J. Heat Mass Transf.* **2017**, *108*, 2534–2557. [CrossRef]
69. Rioux, R.P.; Nolan, E.C.; Li, C.H. A systematic study of pool boiling heat transfer on structured porous surfaces: From nanoscale through microscale to macroscale. *AIP Adv.* **2014**, *4*, 117133. [CrossRef]
70. Jo, B.; Jeon, P.; Yoo, J.; Kim, H. Wide range parametric study for the pool boiling of nano-fluids with a circular plate heater. *Visualization* **2009**, *12*, 37–46. [CrossRef]
71. Patil, C.M.; Kandlikar, S.G. Pool boiling enhancement through microporous coatings selectively electrodeposited on fin tops of open microchannels. *Int. J. Heat Mass Transf.* **2014**, *79*, 816–828. [CrossRef]
72. Jaikumar, A.; Kandlikar, S.G. Enhanced pool boiling heat transfer mechanisms for selectively sintered open microchannels. *Int. J. Heat Mass Transf.* **2015**, *88*, 652–661. [CrossRef]
73. Sarafraz, M.; Hormozi, F.; Peyghambarzadeh, S. Pool boiling heat transfer to aqueous alumina nano-fluids on the plain and concentric circular micro-structured (CCM) surfaces. *Exp. Therm. Fluid Sci.* **2016**, *72*, 125–139. [CrossRef]
74. Shahmoradi, Z.; Etesami, N.; Esfahany, M.N. Pool boiling characteristics of nanofluid on flat plate based on heater surface analysis. *Int. Commun. Heat Mass Transf.* **2013**, *47*, 113–120. [CrossRef]
75. Cheng, L.; Mewes, D.; Luke, A. Boiling phenomena with surfactants and polymeric additives: A state-of-the-art review. *Int. J. Heat Mass Transf.* **2007**, *50*, 2744–2771. [CrossRef]
76. Wasekar, V.M.; Manglik, R.M. A review of enhanced heat transfer in nucleate pool boiling of aqueous surfactant and polymeric solutions. *Enhanc. Heat Transf.* **1999**, *6*, 135–150. [CrossRef]

77. Ciloglu, D.; Bolukbasi, A. A comprehensive review on pool boiling of nanofluids. *Appl. Therm. Eng.* **2015**, *84*, 45–63. [CrossRef]
78. Yu, W.; France, D.M.; Routbort, J.L.; Choi, S.U. Review and comparison of nanofluid thermal conductivity and heat transfer enhancements. *Heat Transf. Eng.* **2008**, *29*, 432–460. [CrossRef]
79. Li, Y.; Tung, S.; Schneider, E.; Xi, S. A review on development of nanofluid preparation and characterization. *Powder Technol.* **2009**, *196*, 89–101. [CrossRef]
80. Özerinç, S.; Kakaç, S.; Yazıcıoğlu, A.G. Enhanced thermal conductivity of nanofluids: A state-of-the-art review. *Microfluid. Nanofluid.* **2010**, *8*, 145–170. [CrossRef]
81. Kleinstreuer, C.; Feng, Y. Experimental and theoretical studies of nanofluid thermal conductivity enhancement: A review. *Nanosc. Res. Lett.* **2011**, *6*, 229. [CrossRef]
82. Ghadimi, A.; Saidur, R.; Metselaar, H. A review of nanofluid stability properties and characterization in stationary conditions. *Int. J. Heat Mass Transf.* **2011**, *54*, 405–4068. [CrossRef]
83. Saidur, R.; Leong, K.; Mohammad, H.A. A review on applications and challenges of nanofluids. *Renew. Sustain. Energy Rev.* **2011**, *15*, 1646–1668. [CrossRef]
84. Ramesh, G.; Prabhu, N.K. Review of thermo-physical properties, wetting and heat transfer characteristics of nanofluids and their applicability in industrial quench heat treatment. *Nanosc. Res. Lett.* **2011**, *6*, 334. [CrossRef] [PubMed]
85. Yu, W.; Xie, H. A review on nanofluids: Preparation, stability mechanisms, and applications. *J. Nanomater.* **2012**, *2012*, 1. [CrossRef]
86. Mahian, O.; Kianifar, A.; Kalogirou, S.A.; Pop, I.; Wongwises, S. A review of the applications of nanofluids in solar energy. *Int. J. Heat Mass Transf.* **2013**, *57*, 582–594. [CrossRef]
87. Sidik, N.A.C.; Mohammed, H.; Alawi, O.A.; Samion, H.; Transfer, M. A review on preparation methods and challenges of nanofluids. *Int. Commun. Heat Mass Transf.* **2014**, *54*, 115–125. [CrossRef]
88. Haddad, Z.; Abid, C.; Oztop, H.F.; Mataoui, A. A review on how the researchers prepare their nanofluids. *Int. J. Therm. Sci.* **2014**, *76*, 168–189. [CrossRef]
89. Shahrul, I.; Mahbubul, I.; Khaleduzzaman, S.; Saidur, R.; Sabri, M. A comparative review on the specific heat of nanofluids for energy perspective. *Renew. Sustain. Energy Rev.* **2014**, *38*, 88–98. [CrossRef]
90. Kasaeian, A.; Eshghi, A.T.; Sameti, M. A review on the applications of nanofluids in solar energy systems. *Renew. Sustain. Energy Rev.* **2015**, *43*, 584–598. [CrossRef]
91. Devendiran, D.K.; Amirtham, V.A. A review on preparation, characterization, properties and applications of nanofluids. *Renew. Sustain. Energy Rev.* **2016**, *60*, 21–40. [CrossRef]
92. Linge, J.M.; Erikson, H.; Kozlova, J.; Sammelselg, V.; Tammeveski, K. Oxygen reduction reaction on electrochemically deposited silver nanoparticles from non-aqueous solution. *Electroanal. Chem.* **2018**, *810*, 129–134. [CrossRef]
93. Qin, L.; Huang, D.; Xu, P.; Zeng, G.; Lai, C.; Fu, Y.; Yi, H.; Li, B.; Zhang, C.; Cheng, M. In-situ deposition of gold nanoparticles onto polydopamine-decorated g-C3N4 for highly efficient reduction of nitroaromatics in environmental water purification. *Colloid Interface Sci.* **2019**, *534*, 357–369. [CrossRef]
94. Cieśliński, J.T.; Krygier, K. Augmentation of the critical heat flux in Water-Al2O3, Water-TiO2 and Water-Cu Nanofluids. In Proceedings of the MATEC Web of Conferences, Chengdu, China, 6–8 September 2014; EDP Sciences: Les Ulis, France, 2014.
95. Truong, B.H. Determination of pool boiling critical heat flux enhancement in nanofluids. In Proceedings of the ASME 2007 International Mechanical Engineering Congress and Exposition, Seattle, WA, USA, 11–15 November 2007; American Society of Mechanical Engineers: New York, NY, USA, 2007.
96. Liu, Y.; Williams, M.G.; Miller, T.J.; Teplyakov, A.V. Nanoparticle layer deposition for highly controlled multilayer formation based on high-coverage monolayers of nanoparticles. *Thin Solid Films* **2016**, *598*, 16–24. [CrossRef] [PubMed]
97. You, S.; Kim, J.; Kim, K. Effect of nanoparticles on critical heat flux of water in pool boiling heat transfer. *Appl. Phys. Lett.* **2003**, *83*, 3374–3376. [CrossRef]
98. Vassallo, P.; Kumar, R.; D'Amico, S. Pool boiling heat transfer experiments in silica–water nano-fluids. *Int. J. Heat Mass Transf.* **2004**, *47*, 407–411. [CrossRef]
99. Bang, I.C.; Chang, S.H. Boiling heat transfer performance and phenomena of Al2O3–water nano-fluids from a plain surface in a pool. *Int. J. Heat Mass Transf.* **2005**, *48*, 2407–2419. [CrossRef]

100. Kim, H.-D.; Kim, J.-B.; Kim, M.-H. Experimental Study on CHF Characteristics of Water-Ti02 Nano-Fluids. *Nucl. Eng. Technol.* **2006**, *38*, 61–68.
101. Kim, S.; Bang, I.C.; Buongiorno, J.; Hu, L. Effects of nanoparticle deposition on surface wettability influencing boiling heat transfer in nanofluids. *Appl. Phys. Lett.* **2006**, *89*, 153107. [CrossRef]
102. Kim, S.J.; Bang, I.C.; Buongiorno, J.; Hu, L. Surface wettability change during pool boiling of nanofluids and its effect on critical heat flux. *Int. J. Heat Mass Transf.* **2007**, *50*, 4105–4116. [CrossRef]
103. Liu, Z.-H.; Xiong, J.-G.; Bao, R. Boiling heat transfer characteristics of nanofluids in a flat heat pipe evaporator with micro-grooved heating surface. *Int. J. Multiph. Flow* **2007**, *33*, 1284–1295. [CrossRef]
104. Coursey, J.S.; Kim, J. Nanofluid boiling: The effect of surface wettability. *Int. J. Heat Fluid Flow* **2008**, *29*, 1577–1585. [CrossRef]
105. Golubovic, M.N.; Hettiarachchi, H.M.; Worek, W.; Minkowycz, W. Nanofluids and critical heat flux, experimental and analytical study. *Appl. Therm. Eng.* **2009**, *29*, 1281–1288. [CrossRef]
106. Kwark, S.M.; Kumar, R.; Moreno, G.; Yoo, J.; You, S.M. Pool boiling characteristics of low concentration nanofluids. *Int. J. Heat Mass Transf.* **2010**, *53*, 972–981. [CrossRef]
107. Huang, C.-K.; Lee, C.-W.; Wang, C.-K. Boiling enhancement by TiO2 nanoparticle deposition. *Int. J. Heat Mass Transf.* **2011**, *54*, 4895–4903. [CrossRef]
108. Sheikhbahai, M.; Esfahany, M.N.; Etesami, N. Experimental investigation of pool boiling of Fe3O4/ethylene glycol–water nanofluid in electric field. *Int. J. Therm. Sci.* **2012**, *62*, 149–153. [CrossRef]
109. Hegde, R.N.; Rao, S.S.; Reddy, R. Experimental studies on CHF enhancement in pool boiling with CuO-water nanofluid. *Heat Mass Transf.* **2012**, *48*, 1031–1041. [CrossRef]
110. Kole, M.; Dey, T. Investigations on the pool boiling heat transfer and critical heat flux of ZnO-ethylene glycol nanofluids. *Appl. Therm. Eng.* **2012**, *37*, 112–119. [CrossRef]
111. Vazquez, D.M.; Kumar, R. Surface effects of ribbon heaters on critical heat flux in nanofluid pool boiling. *Int. Commun. Heat Mass Transf.* **2013**, *41*, 1–9. [CrossRef]
112. Sharma, V.I.; Buongiorno, J.; McKrell, T.J.; Hu, L.W. Experimental investigation of transient critical heat flux of water-based zinc–oxide nanofluids. *Int. J. Heat Mass Transf.* **2013**, *61*, 425–431. [CrossRef]
113. Kim, H.; Kim, E.; Kim, M.H. Effect of nanoparticle deposit layer properties on pool boiling critical heat flux of water from a thin wire. *Int. J. Heat Mass Transf.* **2014**, *69*, 164–172. [CrossRef]
114. Naphon, P.; Thongjing, C. Pool boiling heat transfer characteristics of refrigerant-nanoparticle mixtures. *Int. Commun. Heat Mass Transf.* **2014**, *52*, 84–89. [CrossRef]
115. Sakashita, H. Pressure effect on CHF enhancement in pool boiling of nanofluids. *Nucl. Sci. Technol.* **2016**, *53*, 797–802. [CrossRef]
116. Sarafraz, M.; Kiani, T.; Hormozi, F. Critical heat flux and pool boiling heat transfer analysis of synthesized zirconia aqueous nano-fluids. *Int. Commun. Heat Mass Transf.* **2016**, *70*, 75–83. [CrossRef]
117. Ali, H.M.; Generous, M.M.; Ahmad, F.; Irfan, M. Experimental investigation of nucleate pool boiling heat transfer enhancement of TiO2-water based nanofluids. *Appl. Therm. Eng.* **2017**, *113*, 1146–1151. [CrossRef]
118. Kshirsagar, J.M.; Shrivastava, R. Experimental investigation of nucleate pool boiling characteristics of high concentrated alumina/water nanofluids. *Heat Mass Transf.* **2018**, *54*, 1779–1790. [CrossRef]
119. Kangude, P.; Srivastava, A. Performance of SiO2-water nanofluids for single bubble-based nucleate pool boiling heat transfer. *Int. J. Therm. Sci.* **2019**, *138*, 612–625. [CrossRef]
120. Kathiravan, R.; Kumar, R.; Gupta, A.; Chandra, R. Characterization and pool boiling heat transfer studies of nanofluids. *Heat Transf.* **2009**, *131*, 081902. [CrossRef]
121. Kathiravan, R.; Kumar, R.; Gupta, A.; Chandra, R. Preparation and pool boiling characteristics of copper nanofluids over a flat plate heater. *Int. J. Heat Mass Transf.* **2010**, *53*, 1673–1681. [CrossRef]
122. Zhou, D. Heat transfer enhancement of copper nanofluid with acoustic cavitation. *Int. Commun. Heat Mass Transf.* **2004**, *47*, 3109–3117. [CrossRef]
123. Krishna, K.H.; Ganapathy, H.; Sateesh, G.; Das, S.K. Pool boiling characteristics of metallic nanofluids. *Heat Transf.* **2011**, *133*, 111501. [CrossRef]
124. Kole, M.; Dey, T. Pool boiling heat transfer and critical heat flux enhancement of copper nanoparticles dispersed in distilled water. *Nanofluids* **2014**, *3*, 85–96. [CrossRef]
125. Shi, M.; Shuai, M.; Chen, Z.; Li, Q.; Xuan, Y.-M. Study on pool boiling heat transfer of nano-particle suspensions on plate surface. *Enhanc. Heat Transf.* **2007**, *14*, 223–231. [CrossRef]

126. Cieslinski, J.T.; Kaczmarczyk, T.Z. Pool boiling of water-Al 2 O 3 and water-Cu nanofluids on horizontal smooth tubes. *Nanosc. Res. Lett.* **2011**, *6*, 220. [CrossRef] [PubMed]
127. Goldsmith, A.; Waterman, T.E. *Thermophysical Properties of Solid Materials*; Armour Research Foundation: Chicago, IL, USA, 1960.
128. Touloukian, Y.S. *Thermophysical Properties of High Temperature Solid Materials. Volume 2. Nonferrous Alloys. Part 1. Nonferrous Binary Alloys*; Thermophysical and Electronic Properties Information Analysis Center: New York, NY, USA, 1966.
129. Younglove, B.A. Thermophysical properties of fluids. Argon, I., ethylene, parahydrogen, nitrogen, nitrogen trifluoride, and oxygen. *J. Phys. Chem. Ref. Data* **1982**, *11*. Available online: https://srd.nist.gov/JPCRD/jpcrdS1Vol11.pdf (accessed on 30 July 2020). [CrossRef]
130. Das, S.K.; Putra, N.; Roetzel, W. Pool boiling characteristics of nano-fluids. *Int. Commun. Heat Mass Transf.* **2003**, *46*, 851–862. [CrossRef]
131. Wen, D.; Ding, Y. Experimental investigation into the pool boiling heat transfer of aqueous based γ-alumina nanofluids. *Nanopart. Res.* **2005**, *7*, 265–274. [CrossRef]
132. Soltani, S.; Etemad, S.G.; Thibault, J. Pool boiling heat transfer performance of Newtonian nanofluids. *Heat Mass Transf.* **2009**, *45*, 1555–1560. [CrossRef]
133. Lee, S.; Choi, S.-S.; Li, S.; Eastman, J. Measuring thermal conductivity of fluids containing oxide nanoparticles. *Heat Transf.* **1999**, *121*, 280–289. [CrossRef]
134. Kwak, K.; Kim, C. Viscosity and thermal conductivity of copper oxide nanofluid dispersed in ethylene glycol. *Korea Aust. Rheol. J.* **2005**, *17*, 35–40.
135. Suganthi, K.; Rajan, K. Temperature induced changes in ZnO–water nanofluid: Zeta potential, size distribution and viscosity profiles. *Int. Commun. Heat Mass Transf.* **2012**, *55*, 7969–7980. [CrossRef]
136. Kutateladze, S.S. A hydrodynamic theory of changes in a boiling process under free convection. *Izv. Akad. Nauk Otd. Tekhnicheski Nauk* **1951**, *4*, 529–536.
137. Hong, T.-K.; Yang, H.-S.; Choi, C. Study of the enhanced thermal conductivity of Fe nanofluids. *Appl. Phys. Lett.* **2005**, *97*, 064311. [CrossRef]
138. Quan, X.; Wang, D.; Cheng, P. An experimental investigation on wettability effects of nanoparticles in pool boiling of a nanofluid. *Int. J. Heat Mass Transf.* **2017**, *108*, 32–40. [CrossRef]
139. Bourdon, B.; Rioboo, R.; Marengo, M.; Gosselin, E.; De Coninck, J. Influence of the wettability on the boiling onset. *Langmuir* **2012**, *28*, 1618–1624. [CrossRef] [PubMed]
140. Bourdon, B.; Di Marco, P.; Riobóo, R.; Marengo, M.; De Coninck, J. Enhancing the onset of pool boiling by wettability modification on nanometrically smooth surfaces. *Int. Commun. Heat Mass Transf.* **2013**, *45*, 11–15. [CrossRef]
141. Bourdon, B.; Bertrand, E.; Di Marco, P.; Marengo, M.; Rioboo, R.; De Coninck, J. Wettability influence on the onset temperature of pool boiling: Experimental evidence onto ultra-smooth surfaces. *Adv. Colloid Interface Sci.* **2015**, *221*, 34–40. [CrossRef] [PubMed]
142. Jo, H.; Kim, S.; Kim, H.; Kim, J.; Kim, M.H. Nucleate boiling performance on nano/microstructures with different wetting surfaces. *Nanosc. Res. Lett.* **2012**, *7*, 242. [CrossRef]
143. Kim, S.; Kim, H.; Kim, H.D.; Ahn, H.S.; Kim, M.H.; Kim, J.; Park, G.-C. Experimental investigation of critical heat flux enhancement by micro/nanoscale surface modification in pool boiling. In Proceedings of the ASME 2008 6th International Conference on Nanochannels, Microchannels, and Minichannels, Darmstadt, Germany, 23–5 June 2008; American Society of Mechanical Engineers: New York, NY, USA, 2008.
144. Sun, R.-D.; Nakajima, A.; Fujishima, A.; Watanabe, T.; Hashimoto, K. Photoinduced surface wettability conversion of ZnO and TiO2 thin films. *Phys. Chem. B* **2001**, *105*, 1984–1990. [CrossRef]
145. Takata, Y.; Hidaka, S.; Masuda, M.; Ito, T. Pool boiling on a superhydrophilic surface. *Int. J. Energy Res.* **2003**, *27*, 111–119. [CrossRef]
146. Takata, Y.; Hidaka, S.; Cao, J.; Nakamura, T.; Yamamoto, H.; Masuda, M.; Ito, T. Effect of surface wettability on boiling and evaporation. *Energy* **2005**, *30*, 209–220. [CrossRef]
147. Liaw, S.-P.; Dhir, V. Void fraction measurements during saturated pool boiling of water on partially wetted vertical surfaces. *Heat Transf.* **1989**, *111*, 731–738. [CrossRef]
148. Maeng, Y.H.; Song, S.L.; Lee, J.Y. Unaffectedness of improved wettability on critical heat flux enhancement with TiO2 sputtered surface. *Appl. Phys. Lett.* **2016**, *108*, 074101. [CrossRef]

149. Kim, J.M.; Yu, D.I.; Park, H.S.; Moriyama, K.; Kim, M.H. Smart surface in pool boiling: Thermally-induced wetting transition. *Int. Commun. Heat Mass Transf.* **2017**, *109*, 231–241. [CrossRef]
150. Kim, J.M.; Kim, T.; Yu, D.I.; Kim, M.H.; Moriyama, K.; Park, H.S. Time effect on wetting transition of smart surface and prediction of the wetting transition for critical heat flux in pool boiling. *Int. Commun. Heat Mass Transf.* **2017**, *114*, 735–742. [CrossRef]
151. Kestin, J.; Wakeham, W. A contribution to the theory of the transient hot-wire technique for thermal conductivity measurements. *Phys. A Stat. Mech. Appl.* **1978**, *92*, 102–116. [CrossRef]
152. Wang, X.; Xu, X.; Choi, S.S.U. Thermal conductivity of nanoparticle-fluid mixture. *Thermophys. Heat Transf.* **1999**, *13*, 474–480. [CrossRef]
153. Das, S.K.; Putra, N.; Thiesen, P.; Roetzel, W. Temperature dependence of thermal conductivity enhancement for nanofluids. *Heat Transf.* **2003**, *125*, 567–574. [CrossRef]
154. Xuan, Y.; Li, Q.; Hu, W. Aggregation structure and thermal conductivity of nanofluids. *AIChE* **2003**, *49*, 1038–1043. [CrossRef]
155. Xue, Q.-Z. Model for effective thermal conductivity of nanofluids. *Phys. Lett. A* **2003**, *307*, 313–317. [CrossRef]
156. Xie, H.; Fujii, M.; Zhang, X. Effect of interfacial nanolayer on the effective thermal conductivity of nanoparticle-fluid mixture. *Int. J. Heat Mass Transf.* **2005**, *48*, 2926–2932. [CrossRef]
157. Xue, Q.; Xu, W.-M. A model of thermal conductivity of nanofluids with interfacial shells. *Mater. Chem. Phys.* **2005**, *90*, 298–301. [CrossRef]
158. Hamilton, R.L.; Crosser, O. Thermal conductivity of heterogeneous two-component systems. *Ind. Eng. Chem. Fundam.* **1962**, *1*, 187–191. [CrossRef]
159. Yu, W.; Choi, S. The role of interfacial layers in the enhanced thermal conductivity of nanofluids: A renovated Maxwell model. *Nanopart. Res.* **2003**, *5*, 167–171. [CrossRef]
160. Maxwell, J.C. *A Treatise on Electricity and Magnetism*; Clarendon Press: Oxford, UK, 1881; Volume 1.
161. Kakaç, S.; Pramuanjaroenkij, A. Review of convective heat transfer enhancement with nanofluids. *Int. Commun. Heat Mass Transf.* **2009**, *52*, 3187–3196. [CrossRef]
162. Kamatchi, R.; Venkatachalapathy, S. Parametric study of pool boiling heat transfer with nanofluids for the enhancement of critical heat flux: A review. *Int. J. Therm. Sci.* **2015**, *87*, 228–240. [CrossRef]
163. Kathiravan, R.; Kumar, R.; Gupta, A.; Chandra, R.; Jain, P. Pool boiling characteristics of multiwalled carbon nanotube (CNT) based nanofluids over a flat plate heater. *Int. Commun. Heat Mass Transf.* **2011**, *54*, 1289–1296. [CrossRef]
164. Ganapathy, H.; Sajith, V. Semi-analytical model for pool boiling of nanofluids. *Int. J. Heat Mass Transf.* **2013**, *57*, 32–47. [CrossRef]
165. Ahmed, O.; Hamed, M. Experimental investigation of the effect of particle deposition on pool boiling of nanofluids. *Int. J. Heat Mass Transf.* **2012**, *55*, 3423–3436. [CrossRef]
166. Ahn, H.S.; Kim, J.M.; Kaviany, M.; Kim, M.H. Pool boiling experiments in reduced graphene oxide colloids. Part I–Boiling characteristics. *Int. Commun. Heat Mass Transf.* **2014**, *74*, 501–512. [CrossRef]
167. Kim, H.-D.; Kim, M.-H. Critical heat flux behavior in pool boiling of water-TiO 2 nano-fluids. In Proceedings of the KSME Conference, Taejon, Korea, 3–5 November 2004.
168. Pantzali, M.; Mouza, A.; Paras, S. Investigating the efficacy of nanofluids as coolants in plate heat exchangers (PHE). *Chem. Eng. Sci.* **2009**, *64*, 3290–3300. [CrossRef]
169. Hwang, Y.; Ahn, Y.; Shin, H.; Lee, C.; Kim, G.; Park, H.; Lee, J. Investigation on characteristics of thermal conductivity enhancement of nanofluids. *Curr. Appl. Phys.* **2006**, *6*, 1068–1071. [CrossRef]
170. Zhou, S.-Q.; Ni, R. Measurement of the specific heat capacity of water-based Al_2O_3 nanofluid. *Appl. Phys. Lett.* **2008**, *92*, 093123. [CrossRef]
171. Brinkman, H. The viscosity of concentrated suspensions and solutions. *Chem. Phys.* **1952**, *20*, 571. [CrossRef]
172. Anoop, K.; Kabelac, S.; Sundararajan, T.; Das, S.K. Rheological and flow characteristics of nanofluids: Influence of electroviscous effects and particle agglomeration. *Appl. Phys. Lett.* **2009**, *106*, 034909. [CrossRef]
173. Namburu, P.K.; Kulkarni, D.P.; Misra, D.; Das, D.K. Viscosity of copper oxide nanoparticles dispersed in ethylene glycol and water mixture. *Exp. Therm. Fluid Sci.* **2007**, *32*, 397–402. [CrossRef]
174. Nguyen, C.; Desgranges, F.; Galanis, N.; Roy, G.; Maré, T.; Boucher, S.; Mintsa, H.A. Viscosity data for Al2O3–water nanofluid—hysteresis: Is heat transfer enhancement using nanofluids reliable? *Int. J. Therm. Sci.* **2008**, *47*, 103–111. [CrossRef]

175. Khanafer, K.; Vafai, K. A critical synthesis of thermophysical characteristics of nanofluids. *Int. J. Heat Mass Transf.* **2011**, *54*, 4410–4428. [CrossRef]
176. Chang, T.-B.; Syu, S.-C.; Yang, Y.-K. Effects of particle volume fraction on spray heat transfer performance of Al2O3–water nanofluid. *Int. J. Heat Mass Transf.* **2012**, *55*, 1014–1021. [CrossRef]
177. Utomo, A.T.; Poth, H.; Robbins, P.T.; Pacek, A.W. Experimental and theoretical studies of thermal conductivity, viscosity and heat transfer coefficient of titania and alumina nanofluids. *Int. J. Heat Mass Transf.* **2012**, *55*, 7772–7781. [CrossRef]
178. Vafaei, S.; Purkayastha, A.; Jain, A.; Ramanath, G.; Borca-Tasciuc, T. The effect of nanoparticles on the liquid–gas surface tension of Bi2Te3 nanofluids. *Nanotechnology* **2009**, *20*, 185702. [CrossRef]
179. Kumar, R.; Milanova, D. Effect of surface tension on nanotube nanofluids. *Appl. Phys. Lett.* **2009**, *94*, 073107. [CrossRef]
180. Jeong, Y.H.; Chang, W.J.; Chang, S.H. Wettability of heated surfaces under pool boiling using surfactant solutions and nano-fluids. *Int. J. Heat Mass Transf.* **2008**, *51*, 3025–3031. [CrossRef]
181. Dixon, A.G. Wall and particle-shape effects on heat transfer in packed beds. *Chem. Eng. Commun.* **1988**, *71*, 217–237. [CrossRef]
182. Lin, Y.-J.; Hwang, K.-S. Effects of powder shape and processing parameters on heat dissipation of heat pipes with sintered porous wicks. *Mater. Trans.* **2009**, *50*, 2427–2434. [CrossRef]
183. Fakour, M.; Rahbari, A.; Moghadasi, H.; Rahimipetroudi, I.; Domairry-Ganji, D.; Varmazyar, M. Analytical study of unsteady sedimentation analysis of spherical particle in Newtonian fluid media. *Therm. Sci.* **2018**, *22*, 847–855. [CrossRef]
184. Deng, D.; Tang, Y.; Shao, H.; Zeng, J.; Zhou, W.; Liang, D. Effects of structural parameters on flow boiling performance of reentrant porous microchannels. *Micromech. Microeng.* **2014**, *24*, 065025. [CrossRef]
185. Akbari, E.; Gheitaghy, A.M.; Saffari, H.; Hosseinalipour, S.M. Effect of silver nanoparticle deposition in re-entrant inclined minichannel on bubble dynamics for pool boiling enhancement. *Exp. Therm. Fluid Sci.* **2017**, *82*, 390–401. [CrossRef]
186. Lu, W.-Q.; Fan, Q.-M. Study for the particle's scale effect on some thermophysical properties of nanofluids by a simplified molecular dynamics method. *Eng. Anal. Bound. Elem.* **2008**, *32*, 282–289. [CrossRef]
187. Murshed, S.; Leong, K.; Yang, C. Investigations of thermal conductivity and viscosity of nanofluids. *Int. J. Therm. Sci.* **2008**, *47*, 560–568. [CrossRef]
188. Peng, H.; Ding, G.; Hu, H.; Jiang, W. Effect of nanoparticle size on nucleate pool boiling heat transfer of refrigerant/oil mixture with nanoparticles. *Int. J. Heat Mass Transf.* **2011**, *54*, 1839–1850. [CrossRef]
189. Das, S.K.; Narayan, G.P.; Baby, A.K. Survey on nucleate pool boiling of nanofluids: The effect of particle size relative to roughness. *Nanopart. Res.* **2008**, *10*, 1099–1108. [CrossRef]
190. Phan, H.T.; Caney, N.; Marty, P.; Colasson, S.; Gavillet, J. Surface wettability control by nanocoating: The effects on pool boiling heat transfer and nucleation mechanism. *Int. J. Heat Mass Transf.* **2009**, *52*, 5459–5471. [CrossRef]
191. Hu, Y.; Li, H.; He, Y.; Liu, Z.; Zhao, Y. Effect of nanoparticle size and concentration on boiling performance of SiO_2 nanofluid. *Int. J. Heat Mass Transf.* **2017**, *107*, 820–828. [CrossRef]
192. Kim, H.; Kim, M. Experimental study of the characteristics and mechanism of pool boiling CHF enhancement using nanofluids. *Heat Mass Transf.* **2009**, *45*, 991–998. [CrossRef]
193. Lee, J.H.; Lee, T.; Jeong, Y.H. Experimental study on the pool boiling CHF enhancement using magnetite-water nanofluids. *Int. J. Heat Mass Transf.* **2012**, *55*, 2656–2663. [CrossRef]
194. Jung, J.-Y.; Kim, E.S.; Kang, Y.T. Stabilizer effect on CHF and boiling heat transfer coefficient of alumina/water nanofluids. *Int. J. Heat Mass Transf.* **2012**, *55*, 1941–1946. [CrossRef]
195. Liu, Z.-H.; Yang, X.-F.; Xiong, J.-G. Boiling characteristics of carbon nanotube suspensions under sub-atmospheric pressures. *Int. J. Therm. Sci.* **2010**, *49*, 1156–1164. [CrossRef]
196. Kim, J.; Kim, K.; You, S. Pool boiling heat transfer in saturated nanofluids. In Proceedings of the ASME 2004 International Mechanical Engineering Congress and Exposition, Anaheim, CA, USA, 13–19 November 2004; American Society of Mechanical Engineers: New York, NY, USA, 2004.

197. Moreno, G.; Oldenburg, S.J.; You, S.M.; Kim, J.H. Pool boiling heat transfer of alumina-water, zinc oxide-water and alumina-water+ ethylene glycol nanofluids. In Proceedings of the ASME 2005 Summer Heat Transfer Conference collocated with the ASME 2005 Pacific Rim Technical Conference and Exhibition on Integration and Packaging of MEMS, NEMS, and Electronic Systems, San Francisco, CA, USA, 17–22 July 2005; American Society of Mechanical Engineers: New York, NY, USA, 2005.
198. Ham, J.; Kim, H.; Shin, Y.; Cho, H. Experimental investigation of pool boiling characteristics in Al2O3 nanofluid according to surface roughness and concentration. *Int. J. Therm. Sci.* **2017**, *114*, 86–97. [CrossRef]
199. Hiswankar, S.; Kshirsagar, J. Determination of critical heat flux in pool boiling using ZnO nanofluids. *Int. J. Eng. Res. Technol.* **2013**, *2*, 2091–2095.
200. Kim, H.D.; Kim, J.; Kim, M.H. Experimental studies on CHF characteristics of nanofluids at pool boiling. *Int. J. Multiph. Flow* **2007**, *33*, 691–706. [CrossRef]
201. Prakash, C.J.; Prasanth, R. Enhanced boiling heat transfer by nano structured surfaces and nanofluids. *Renew. Sustain. Energy Rev.* **2018**, *82*, 4028–4043. [CrossRef]
202. Sulaiman, M.Z.; Matsuo, D.; Enoki, K.; Okawa, T. Systematic measurements of heat transfer characteristics in saturated pool boiling of water-based nanofluids. *Int. J. Heat Mass Transf.* **2016**, *102*, 264–276. [CrossRef]
203. Kim, H.; Kim, J.; Kim, M.H. Effect of nanoparticles on CHF enhancement in pool boiling of nano-fluids. *Int. J. Heat Mass Transf.* **2006**, *49*, 5070–5074. [CrossRef]
204. Kim, H.D.; Kim, M.H. Effect of nanoparticle deposition on capillary wicking that influences the critical heat flux in nanofluids. *Appl. Phys. Lett.* **2007**, *91*, 014104. [CrossRef]
205. Kim, H.; Ahn, H.S.; Kim, M.H. On the mechanism of pool boiling critical heat flux enhancement in nanofluids. *Heat Transf.* **2010**, *132*, 061501. [CrossRef]
206. Suriyawong, A.; Wongwises, S. Nucleate pool boiling heat transfer characteristics of TiO_2–water nanofluids at very low concentrations. *Exp. Therm. Fluid Sci.* **2010**, *34*, 992–999. [CrossRef]
207. Chopkar, M.; Das, A.; Manna, I.; Das, P. Pool boiling heat transfer characteristics of ZrO_2–water nanofluids from a flat surface in a pool. *Heat Mass Transf.* **2008**, *44*, 999–1004. [CrossRef]
208. Jung, J.-Y.; Kim, E.S.; Nam, Y.; Kang, Y.T. The study on the critical heat flux and pool boiling heat transfer coefficient of binary nanofluids (H_2O/LiBr+ Al_2O_3). *Int. J. Refrig.* **2013**, *36*, 1056–1061. [CrossRef]
209. Lotfi, H.; Shafii, M. Boiling heat transfer on a high temperature silver sphere in nanofluid. *Int. J. Therm. Sci.* **2009**, *48*, 2215–2220. [CrossRef]
210. Mori, S.; Suazlan, M.; Okuyama, K. The CHF enhancement of a saturated pool boiling using nano-fluids and honeycomb porous plates. In Proceedings of the Annual Meeting of the Atomic Energy Society of Japan, Kyoto University, Kyoto, Japan, 30 May 2014.
211. Mori, S.; Mt Aznam, S.; Yanagisawa, R.; Okuyama, K. CHF enhancement by honeycomb porous plate in saturated pool boiling of nanofluid. *Nucl. Sci. Technol.* **2016**, *53*, 1028–1035. [CrossRef]
212. Park, K.-J.; Jung, D.; Shim, S.E. Nucleate boiling heat transfer in aqueous solutions with carbon nanotubes up to critical heat fluxes. *Int. J. Multiph. Flow* **2009**, *35*, 525–532. [CrossRef]
213. Truong, B.; Hu, L.-W.; Buongiorno, J.; McKrell, T. Modification of sandblasted plate heaters using nanofluids to enhance pool boiling critical heat flux. *Int. J. Heat Mass Transf.* **2010**, *53*, 85–94. [CrossRef]
214. Choi, S.U. Nanofluids: From vision to reality through research. *Heat Transf.* **2009**, *131*, 033106. [CrossRef]
215. Milanova, D.; Kumar, R.; Kuchibhatla, S.; Seal, S. Heat transfer behavior of oxide nanoparticles in pool boiling experiment. In Proceedings of the ASME 4th International Conference on Nanochannels, Microchannels, and Minichannels, Limerick, Ireland, 19–21 June 2006; American Society of Mechanical Engineers: New York, NY, USA, 2006.
216. Milanova, D.; Kumar, R. Heat transfer behavior of silica nanoparticles in pool boiling experiment. *Heat Transf.* **2008**, *130*, 042401. [CrossRef]
217. Ahmed, O.; Hamed, M.S. Effects of acidity and method of preparation on nucleate pool boiling of nanofluids. *Heat Transf. Eng.* **2012**, *33*, 1148–1155. [CrossRef]
218. Wu, W.; Yang, Y. Enhanced boiling heat transfer by surfactant additives. *Pool Extern. Flow Boil.* **1992**, *1992*, 361–366.
219. Jeong, Y.H.; Chang, S.H.; Baek, W.-P. Critical heat flux experiments on the reactor vessel wall using 2-D slice test section. *Nucl. Technol.* **2005**, *152*, 162–169. [CrossRef]
220. Jeong, J.; Kwon, Y. Effects of ultrasonic vibration on subcooled pool boiling critical heat flux. *Heat Mass Transf.* **2006**, *42*, 1155–1161. [CrossRef]

221. Giancane, G.; Ruland, A.; Sgobba, V.; Manno, D.; Serra, A.; Farinola, G.M.; Omar, O.H.; Guldi, D.M.; Valli, L. Aligning single-walled carbon nanotubes by means of langmuir–blodgett film deposition: Optical, morphological, and photo-electrochemical studies. *Adv. Funct. Mater.* **2010**, *20*, 2481–2488. [CrossRef]
222. Hotze, E.M.; Phenrat, T.; Lowry, G.V. Nanoparticle aggregation: Challenges to understanding transport and reactivity in the environment. *Environ. Qual.* **2010**, *39*, 1909–1924. [CrossRef]
223. Lambert, K.; Capek, R.K.; Bodnarchuk, M.I.; Kovalenko, M.V.; Van Thourhout, D.; Heiss, W.; Hens, Z. Langmuir–Schaefer deposition of quantum dot multilayers. *Langmuir* **2010**, *26*, 7732–7736. [CrossRef]
224. Kim, H. Enhancement of critical heat flux in nucleate boiling of nanofluids: A state-of-art review. *Nanosc. Res. Lett.* **2011**, *6*, 415. [CrossRef]
225. Kwark, S.-M.; Amaya, M.; Moon, H.-J.; You, S.-M. Effect of soluble additives, boric acid (H_3BO_3) and salt (NaCl), in pool boiling heat transfer. *Nucl. Eng. Technol.* **2011**, *43*, 195–204. [CrossRef]
226. Harish, G.; Emlin, V.; Sajith, V. Effect of surface particle interactions during pool boiling of nanofluids. *Int. J. Therm. Sci.* **2011**, *50*, 2318–2327. [CrossRef]
227. Wen, D.; Corr, M.; Hu, X.; Lin, G. Boiling heat transfer of nanofluids: The effect of heating surface modification. *Int. J. Therm. Sci.* **2011**, *50*, 480–485. [CrossRef]
228. Jung, J.-Y.; Kim, H.; Kim, M.H. Effect of ionic additive on pool boiling critical heat flux of titania/water nanofluids. *Heat Mass Transf.* **2013**, *49*, 1–10. [CrossRef]
229. Saffari, H.; Moghadasi, H.; Malekian, N.; Hosseinalipour, S.M. Modeling heat transf. in nucleate pool boiling: Influence of nucleation sites density, contact angle and prandtl number. In Proceedings of the Third International Conference on Innovation and Research in Engineering Sciences, Tbilisi, Gerorgia, 21 July 2019.
230. Kolev, N.I. How accurately can we predict nucleate boiling. In *Multiphase Flow Dynamics*; Springer: Berlin/Heidelberg, Germany, 2007; Volume 2, pp. 439–470.
231. Gheitaghy, A.M.; Saffari, H.; Arshadi, S.S.; Tabatabaei, S.S. Prediction of pool boiling angle effect on isolated bubble. *Heat. Trans. Res.* **2018**, *49*, 423–435. [CrossRef]
232. Barber, J.; Brutin, D.; Tadrist, L. A review on boiling heat transfer enhancement with nanofluids. *Nanosc. Res. Lett.* **2011**, *6*, 280. [CrossRef]
233. Park, S.D.; Won Lee, S.; Kang, S.; Bang, I.C.; Kim, J.H.; Shin, H.S.; Lee, D.W.; Won Lee, D. Effects of nanofluids containing graphene/graphene-oxide nanosheets on critical heat flux. *Appl. Phys. Lett.* **2010**, *97*, 023103. [CrossRef]
234. Ahn, H.S.; Kim, J.M.; Park, C.; Jang, J.-W.; Lee, J.S.; Kim, H.; Kaviany, M.; Kim, M.H. A novel role of three dimensional graphene foam to prevent heater failure during boiling. *Sci. Rep.* **2013**, *3*, 1960. [CrossRef]
235. Ahn, H.S.; Kim, J.M.; Kim, M.H. Experimental study of the effect of a reduced graphene oxide coating on critical heat flux enhancement. *Int. J. Heat Mass Transf.* **2013**, *60*, 763–771. [CrossRef]
236. Zuber, N. On the stability of boiling heat transfer. *Trans. Am. Soc. Mech. Engrs.* **1958**, *80*. Available online: https://www.osti.gov/biblio/4326542 (accessed on 30 July 2020).
237. Haramura, Y.; Katto, Y. A new hydrodynamic model of critical heat flux, applicable widely to both pool and forced convection boiling on submerged bodies in saturated liquids. *Int. J. Heat Mass Transf.* **1983**, *26*, 389–399. [CrossRef]
238. Rohsenow, W.M.; Griffith, P. *Correlation of Maximum Heat Flux Data for Boiling of Saturated Liquids*; Massachusetts Institute of Technology, Division of Industrial Cooperation: Cambridge, MA, USA, 1955.
239. Yagov, V.V. Is a crisis in pool boiling actually a hydrodynamic phenomenon? *Int. J. Heat Mass Transf.* **2014**, *73*, 265–273. [CrossRef]
240. Theofanous, T.; Dinh, T.-N.; Tu, J.; Dinh, A. The boiling crisis phenomenon: Part II: Dryout dynamics and burnout. *Exp. Therm. Fluid Sci.* **2002**, *26*, 793–810. [CrossRef]
241. Zuber, N. *Hydrodynamic Aspects of Heat Transfer*; UCLA: Los Angeles, CA, USA, 1959.
242. Lienhard, J.; Dhir, V. Hydrodynamic prediction of peak pool-boiling heat fluxes from finite bodies. *Heat Transf.* **1973**, *95*, 152–158. [CrossRef]
243. Dinh, T.; Thu, J.; Theofanous, T. Burnout in high heat flux boiling: The hydrodynamic and physico-chemical factors. In Proceedings of the 42nd AIAA Aerospace Sciences Meeting and Exhibit, Reno, Nevada, 5–8 January 2004.
244. Sadasivan, P.; Chappidi, P.; Unal, C.; Nelson, R. Possible mechanisms of macrolayer formation. *Int. Commun. Heat Mass Transf.* **1992**, *19*, 801–815. [CrossRef]

245. Wang, C.; Dhir, V. Effect of surface wettability on active nucleation site density during pool boiling of water on a vertical surface. *Heat Transf.* **1993**, *115*, 659–669. [CrossRef]
246. Yagov, V. A physical model and calculation formula for critical heat fluxes with nucleate pool boiling of liquids. *Therm. Eng.* **1988**, *35*, 333–339.
247. Ha, S.J.; No, H.C. A dry-spot model of critical heat flux in pool and forced convection boiling. *Int. J. Heat Mass Transf.* **1998**, *41*, 303–311. [CrossRef]
248. Ha, S.J.; No, H.C. A dry-spot model of critical heat flux applicable to both pool boiling and subcooled forced convection boiling. *Int. J. Heat Mass Transf.* **2000**, *43*, 241–250. [CrossRef]
249. Chung, H.J.; No, H.C. A nucleate boiling limitation model for the prediction of pool boiling CHF. *Int. J. Heat Mass Transf.* **2007**, *50*, 2944–2951. [CrossRef]
250. Xiao, B.; Yu, B. A fractal model for critical heat flux in pool boiling. *Int. J. Therm. Sci.* **2007**, *46*, 426–433. [CrossRef]
251. Van Ouwerkerk, H. Burnout in pool boiling the stability of boiling mechanisms. *Int. J. Heat Mass Transf.* **1972**, *15*, 25–34. [CrossRef]
252. Liang, G.; Mudawar, I. Pool boiling critical heat flux (CHF)–Part 1: Review of mechanisms, models, and correlations. *Int. J. Heat Mass Transf.* **2018**, *117*, 1352–1367. [CrossRef]
253. Kam, D.H.; Jeong, Y.H.; Cheon, H. A heat transfer model development for CHF prediction with consideration of dry patch characteristics. *Int. J. Heat Mass Transf.* **2020**, *148*, 25–34. [CrossRef]
254. Theofanous, T.; Tu, J.; Dinh, A.; Dinh, T.-N. The boiling crisis phenomenon: Part I: Nucleation and nucleate boiling heat transfer. *Exp. Therm. Fluid Sci.* **2002**, *26*, 775–792. [CrossRef]
255. Jung, J.; Kim, S.J.; Kim, J. Observations of the critical heat flux process during pool boiling of FC-72. *Heat Transf.* **2014**, *136*, 041501. [CrossRef]
256. Theofanous, T.G.; Dinh, T.-N. High heat flux boiling and burnout as microphysical phenomena: Mounting evidence and opportunities. *Multiph. Sci. Technol.* **2006**, *18*. [CrossRef]
257. Gupta, S. Capillary action in narrow and wide tubes—A unified approach. *Metrologia* **2004**, *41*, 361. [CrossRef]
258. Chu, I.-C.; No, H.C.; Song, C.-H.; Euh, D.J. Observation of critical heat flux mechanism in horizontal pool boiling of saturated water. *Nucl. Eng. Des.* **2014**, *279*, 189–199. [CrossRef]
259. Choi, J.Y.; No, H.C.; Kim, J. Development of a dry patch model for critical heat flux prediction. *Int. J. Heat Mass Transf.* **2016**, *100*, 386–395. [CrossRef]
260. Kim, D.E.; Song, J.; Kim, H. Simultaneous observation of dynamics and thermal evolution of irreversible dry spot at critical heat flux in pool boiling. *Int. J. Heat Mass Transf.* **2016**, *99*, 409–424. [CrossRef]
261. Chu, I.-C.; No, H.C.; Song, C.-H. Visualization of boiling structure and critical heat flux phenomenon for a narrow heating surface in a horizontal pool of saturated water. *Int. J. Heat Mass Transf.* **2013**, *62*, 142–152. [CrossRef]
262. Galloway, J.; Mudawar, I. CHF mechanism in flow boiling from a short heated wall—I. Examination of near-wall conditions with the aid of photomicrography and high-speed video imaging. *Int. J. Heat Mass Transf.* **1993**, *36*, 2511–2526. [CrossRef]
263. Galloway, J.; Mudawar, I. CHF mechanism in flow boiling from a short heated wall—II. Theoretical CHF model. *Int. J. Heat Mass Transf.* **1993**, *36*, 2527–2540. [CrossRef]
264. Mudawar, I.; Howard, A.H.; Gersey, C.O. An analytical model for near-saturated pool boiling critical heat flux on vertical surfaces. *Int. J. Heat Mass Transf.* **1997**, *40*, 2327–2339. [CrossRef]
265. Howard, A.H.; Mudawar, I. Orientation effects on pool boiling critical heat flux (CHF) and modeling of CHF for near-vertical surfaces. *Int. J. Heat Mass Transf.* **1999**, *42*, 1665–1688. [CrossRef]
266. Kim, Y.; Kim, S.; Kim, J.; Noh, S.; Suh, K.; Rempe, J.; Cheung, F.; Kim, S. Visualization of boiling phenomena in inclined rectangular gap. *Int. J. Multiph. Flow* **2005**, *31*, 618–642. [CrossRef]
267. Zhong, D.; Meng, J.A.; Li, Z.; Guo, Z. Critical heat flux for downward-facing saturated pool boiling on pin fin surfaces. *Int. J. Heat Mass Transf.* **2015**, *87*, 201–211. [CrossRef]
268. Zhang, H.; Mudawar, I.; Hasan, M.M. Experimental assessment of the effects of body force, surface tension force, and inertia on flow boiling CHF. *Int. J. Heat Mass Transf.* **2002**, *45*, 4079–4095. [CrossRef]
269. Zhang, H.; Mudawar, I.; Hasan, M.M. Flow boiling CHF in microgravity. *Int. J. Heat Mass Transf.* **2005**, *48*, 3107–3118. [CrossRef]
270. Konishi, C.; Mudawar, I. Review of flow boiling and critical heat flux in microgravity. *Int. J. Heat Mass Transf.* **2015**, *80*, 469–493. [CrossRef]

271. Guan, C.-K.; Klausner, J.F.; Mei, R. A new mechanistic model for pool boiling CHF on horizontal surfaces. *Int. J. Heat Mass Transf.* **2011**, *54*, 3960–3969. [CrossRef]
272. Rajvanshi, A.; Saini, J.; Prakash, R. Investigation of macrolayer thickness in nucleate pool boiling at high heat flux. *Int. J. Heat Mass Transf.* **1992**, *35*, 343–350. [CrossRef]